SYNTHETIC APERTURE RADAR (SAR) IMAGE COMPRESSION USING THE WAVELET TRANSFORM

YING LI

Synthetic Aperture Radar (SAR) Image Compression Using the Wavelet Transform

By

©Ying Li

A thesis

submitted to the School of Graduate Studies

in partial fulfillment of the requirements for

the degree of Master of Engineering

Faculty of Engineering and Applied Sciences

Memorial University of Newfoundland

August, 1997

St.John's Newfoundland Canada A1B 3X5

National Library of Canada
Acquisitions and Bibliographic Services
395 Wellington Street
Ottawa ON K1A 0N4
Canada

Bibliothèque nationale du Canada
Acquisitions et services bibliographiques
395, rue Wellington
Ottawa ON K1A 0N4
Canada

Your file Votre référence

Our file Notre référence

0-612-34199-2

Canada

Abstract

Along with the success of Synthetic Aperture Radar (SAR) imaging systems and the large amount of data which they routinely produce, SAR image compression has begun to attract the attention of researchers seeking solutions for efficient image transmission and storage. In this thesis, two key characteristics of SAR images, namely their speckle noise and varied image contents are addressed. We develop a selective soft-thresholding method and a multi-rate compression scheme to compress SAR images more efficiently, using the wavelet transform to accomplish both the noise smoothing and image compression tasks.

We initially approach the SAR image compression problem by studying the effects of SAR image characteristics using standard compression techniques, such as Joint Photographic Expert Group (JPEG) method, the Efficient Pyramidal Image Coder (EPIC) and the Embedded Zerotree Wavelet (EZW) coder. We find that speckle noise tends to break the inter-pixel correlation in SAR images and thus has negative effects on compression. In order to compress SAR images more efficiently, we need to smooth speckle noise

and to enhance inter-pixel correlation prior to image compression. To this end, we develop a selective soft-thresholding method which refines Donoho's overall soft-thresholding method. The proposed method makes use of the correlation structure of wavelet coefficients to select edge coefficients in the wavelet domain and then protects them from soft-thresholding. Test results show that this method can smooth speckle noise and preserve edges and hence enable more efficient compression.

Another issue in SAR image compression is concerned with the varied scene contents within large-size SAR images. We propose a multi-rate compression scheme on top of the EZW algorithm. This scheme partitions an image into several regions in the wavelet domain. Each region is assigned a different bit budget according to the relative importance of the information each region contains. A highlighted region can be encoded with higher accuracy and only the major structures in the background regions transmitted. This scheme, when combined with the selective soft-thresholding method, can provide better visual quality for the highlighted regions; major structures in the background can be easily picked up while finer details and speckle noise corrupted coefficients are eliminated at low bit-per-pixel rates.

This work demonstrates applications of the wavelet transform in SAR image processing and compression. Many issues for future work are also recommended.

Acknowledgment

I sincerely acknowledge and thank my supervisor Professor Cecilia Moloney for all her involvement, patience, criticisms and constant encouragement for my work for the whole duration of my program here. I thank The School of Graduate Studies of Memorial University, the Faculty of Engineering, the Associate Dean of Engineering (Graduate Studies) and his office for the financial support provided.

The SAR data and images are used and presented with the permission of the Canada Center for Remote Sensing (CCRS). I acknowledge with thanks the use of source code for the EPIC (provided by E.H. Adelso and E.P. Simoncelli) and EZW (provided by A. Said and W.A. Pearlman), obtained from their respective web sites which have been used in the research only purposes.

I also thank all of my fellow graduate students in the Faculty of Engineering for many sweet memories.

Finally, I deeply acknowledge the constant support of my husband and our parents.

Contents

List of Figures

List of Tables

Chapter 1

Introduction

1.1 General

Image compression is important for the storage and transmission of Synthetic Aperture Radar (SAR) images. The success of the operating SAR systems, such as the Seasat-A SAR, the Shuttle Imaging Radar (SIR-A and SIR-B) missions, together with the recent launch of the Canadian Radarsat satellite, and numerous airborne SAR systems, has stimulated considerable interests in both airborne and space-borne SAR as a remote sensing tool. However, the large amount of data collection planned for current and future SAR missions poses a severe problem for existing data handling, archiving, and distribution systems. Thus, there is a necessity of SAR image compression for effective storage and transmission of these images.

To alleviate the conflict between the increasing demands of SAR data transmission and a need for viable high rate data transmission channels, many techniques have been proposed to meet the anticipated data flow re-

quirements. Compression of image data could reduce the data volume and significantly decrease both the transmission and archive costs, and thus provides a solution to this problem.

1.2 Motivation

The goal of this thesis is to study how SAR images can be efficiently compressed for data storage and transmission purposes. SAR images can be used in a myriad of earth observation applications covering areas in global environment monitoring, mapping, charting, and land use planning. There is also the area of natural resource management, including forestry, agriculture, water quality monitoring and wildlife habitat management. With such a diverse set of applications comes a wide variety of system requirements: the challenge of including SAR image compression in a system is to preserve sufficient information content of the imagery, while providing compression ratios large enough to allow high data transmission rates and archival ratios.

Various image data compression algorithms have been proposed exploiting the spatial and/or spectral correlation existing in images which achieve the compression goal by decorrelation. But these algorithms are less suitable for use with the images of coherent image systems, such as SAR, due to the special characteristics of these images, since most of these algorithms only work successfully for noise-free images.

Although the nature and characteristics of SAR images have been well

studied, the problem of compressing SAR images has not been studied in depth by many researchers. Moreover, the effect of SAR image characteristics on SAR image compression has not been explicitly investigated.

1.3 Problem definition

In order to attain good compression results for SAR images, SAR image data characteristics must be taken into account. This thesis will address the effects of two key characteristics of SAR images, namely their speckle noise and their wide dynamic range, on SAR image compression.

Speckle noise contamination of SAR images is an important data characteristic that needs to be considered in SAR image compression. Speckle is an inherent phenomenon in coherent imaging systems [21]. As we will see later in Chapter 4, speckle noise not only obscures image scene contents, but also reduces image compression performance by weakening or breaking the inter-pixel correlation. Consequently, in order to compress SAR images more efficiently, it is desirable to reduce speckle noise prior to compression.

Another consideration in designing SAR image compression algorithms is that SAR images are usually of large size; as such these different regions may exhibit a variety of information content which are of differing levels of interest for different users. Therefore, a multiresolution or multirate compression scheme may be preferred in these situations. Certain user-defined regions could be compressed with significant image detail while other regions may

be represented more frugally, simply providing basic background information. This scheme can make full use of available transmission resources and reduce response time as well.

In this research, a two-step approach to SAR image compression is taken. First, the effect of speckle noise on image compression is investigated. A wavelet domain speckle noise reduction algorithm is then proposed to produce less noisy SAR images which are more compressible. Second, a multi-rate compression scheme is implemented to cope with the wide dynamic range of SAR images and to enhance progressive transmission capability.

1.4 Approach to the solution

The goal of compression of SAR images can be achieved by two approaches:

- lossless compression: no information is lost due to compression, i.e., the recovered image is identical to the original image;
- lossy compression: some information is lost due to compression, i.e., the image can only be recovered with some degradation.

Many SAR image compression algorithms are designed for lossless compression [43, 51]. However, as we will discuss later, for typical SAR images, lossless compression algorithms usually achieve compression ratios no greater than 3:1 [40]. The maximum compression ratio is bounded by the instrument noise introduced during image generation. While this compression ratio is

tolerable for data storage, it is far from sufficient for transmission purposes.

Lossy algorithms are more likely to be required for higher compression. Some researchers have adopted algorithms successfully used for optical images to compress SAR images [10, 36]. But these algorithms perform less effectively for SAR image compression. We conclude that this is because of the peculiar characteristics possessed by SAR images. In order to cope with these characteristics, especially the speckle noise phenomena, two different approaches can be followed:

- direct approach: compress speckled SAR images directly;
- indirect approach: compress pre-processed SAR images.

The direct approach operates on SAR images without any prior processing such as edge enhancement or speckle smoothing. These direct compression methods must be deliberately designed to account for the effects of speckle noise. Since speckle noise tends to weaken the inter-pixel correlation in SAR images, effective compression methods need to re-build the inter-pixel correlation by reference to a model of speckle and its statistical distribution. No compression algorithm belonging to this category has been reported in the literature to date. In fact, we are convinced that if such a method were to succeed in re-building the inter-pixel correlation, it would also be a good speckle filter itself.

The indirect approach, on the other hand, operates by compressing pre-processed images. These pre-processed images, which may be the results

of speckle smoothing, are easier to compress as we will demonstrate in this thesis. Or they may be pre-segmented according to intensity, texture or scene contents. The purpose of this pre-processing is to assist in dealing with the large size of SAR images and the variety of SAR image contents. The major disadvantage of methods following this approach is the computational cost for the pre-processing operations. But we consider the indirect approach to be practical because:

- Speckle reduction is usually required before many other image analysis operations;
- Many speckle filters have been designed which can be used;
- There are many successful image compression algorithms available for optical or noise-free images.

Thus, the indirect compression approach will be a combination of the pre-processing of SAR images, such as speckle smoothing, and a conventional compression algorithm with some SAR-specific modifications. We will follow this approach in this thesis.

Speckle noise reduction is usually performed in the spatial domain. In this thesis, we attempt to smooth speckle noise in the wavelet domain. The frequently-used multiplicative speckle model is assumed. After a logarithmic operation, speckle noise is converted into additive noise which remains uncorrelated in the wavelet domain. Because intra-correlation exists between

neighbor coefficients at the same scale and inter-band correlation between coefficients in adjacent scales, we can make use of this short term correlation to distinguish edge coefficients from noise coefficients. Thus wavelet coefficient soft-thresholding can be performed on noise coefficients in such a way that the speckle noise is removed while major structures are preserved.

In addition, a multirate SAR image compression scheme is implemented based on the embedded zerotree wavelet coding algorithm [44] to facilitate efficient transmission of large SAR images with user-emphasized regions. The selection of these regions and the setting of appropriate parameters for each of these regions is beyond the scope of this thesis. Here we assume these regions have already been specified. Using wavelet domain image partition. the highlighted regions are encoded with high bit rates to retain adequate image details, and only large structures are selected from the other regions and are encoded with low bit rates to provide background information. The various data streams which correspond to different regions are recombined at the receiver and used to provide the viewer with a multiresolution SAR image.

In this thesis, we utilize the wavelet transform to accomplish the noise reduction and image compression tasks. A bi-orthogonal wavelet transform transform is used throughout this thesis.

1.5 Outline of thesis

This thesis is organized into 8 chapters. The literature review spans two chapters. Chapter 2 is the first part of the literature review, mainly addressing several topics related to SAR imaging systems, including the SAR imaging mechanism, speckle models and spatial domain speckle filters. Chapter 3 is the second part of literature review, covering the fundamental theory of the wavelet transform and its applications in image compression and processing, including the embedded zerotree wavelet coefficient compression algorithm and the wavelet coefficient soft-thresholding method. A brief review of the available image compression algorithms for remotely sensed images is also provided in this chapter. In Chapter 4, SAR image compression using conventional algorithms is evaluated and the effect of speckle noise on SAR image compression is studied. A speckle noise reduction method using selective wavelet coefficient soft-thresholding is presented in Chapter 5, together with test results on simulated speckled images. Chapter 6 describes the implementation of the modified multirate EZW algorithm on a trial basis. The results of Chapter 5 and Chapter 6 are corroborated in Chapter 7 by test results of both methods on real airborne SAR images together with discussion of the methods and results. The speckle smoothing performance of the proposed method, the effect of speckle smoothing on image compression and the effectiveness of the multirate compression scheme are evaluated using both quantitative and qualitative measures. Finally, conclusions and recom-

mendations for future work are given in Chapter 8.

Chapter 2

Synthetic Aperture Radar Images and Speckle Filters

2.1 Introduction

As the first part of the literature review, this chapter reviews several topics related to Synthetic Aperture Radar (SAR) imaging systems, the nature and characteristics of speckle noise, and speckle filters. SAR is an active imaging system widely used in remote sensing applications. SAR systems are characterized by their high image resolution and all-weather operating ability, but SAR images also suffer from the notorious speckle noise, a chaotic phenomenon that results from coherent imaging [21]. Speckle noise can obscure scene content and strongly reduce capabilities for object detection and recognition. In addition, as we will see later, speckle noise is also an obstacle to image compression. Thus speckle smoothing is usually the first step in SAR image processing. This chapter briefly describes the multiplicative speckle model and several speckle filters based on this model.

2.2 Fundamental Theory of Synthetic Aperture Radar (SAR)

2.2.1 What is SAR

A radar system illuminates an area with microwave pulses and records the strength and travel-time of the returned signals. This allows the distance (or range) of the reflecting objects to be determined. As in an optical instrument, the resolution of such a system is affected by the size of the aperture: a larger aperture gives a finer resolution. However, the aperture size can not be increased beyond some practical limits. Therefore, we should search for other solutions in order to generate high resolution images.

A synthetic aperture radar (SAR) is a coherent system in that it retains both the phase and magnitude of the backscattered echo signal. It can be attached to a moving platform, either a satellite or an aircraft. As the radar moves, pulses are transmitted at a fixed repetition rate. the return echoes pass through the receiver and are recorded in an 'echo store'. Because the radar is moving relative to the ground, the returned echoes are Doppler-shifted (negatively as the radar approaches a target; positively as it moves away). Comparing the Doppler-shifted frequencies to a reference frequency allows many returned signals to be "focused" on a single point, effectively increasing the length of the antenna that is imaging that particular point. This is typically performed digitally in a ground computer by compensating for the quadratic phase characteristic associated with what is effectively near

field imaging by the long synthetic array. The net effect is that the SAR system is capable of achieving a resolution independent of the sensor altitude. This characteristic makes the SAR an extremely valuable instrument for space observation. For a more comprehensive explanation of the theory of SAR systems, the reader is directed to [13, 53].

2.2.2 Characteristics of SAR Systems and SAR Applications

Synthetic aperture radar is now a mature technology used to generate radar images in which fine detail can be resolved. Besides high image resolution, SARs provide unique capabilities as an imaging tool. Because they provide their own illumination (the radar pulses), they can image at any time of day or night, regardless of optical illumination. And because the radar wavelengths are much longer than those of visible or infra-red light, SARs can also "see" through cloudy and dusty conditions that visible and infra-red instruments cannot.

The disadvantage of SAR is the high noise to signal ratio - typically 1:1 as compared to 1:1000 for optical images[56]. This speckle noise is an intrinsic part of any image formation process which uses coherent imaging. It implies that standard techniques for processing optical data may not work when applied to SAR images.

SAR is an increasingly important technique for remote sensing. The radar can by carried on an aircraft or a satellite achieving resolutions of up to 3m

per pixel from aircraft and 10m per pixel from space [53]. This is easily good enough to monitor large scale features like changes in agriculture or forestry, or ice in the oceans. As a result, SAR has become an important tool for geophysical monitoring. Applications of SAR include classification of land use, crop monitoring, tropical deforestation monitoring, ice floe detection or tracking, oil slick detection, and other change detection tasks.

2.3 Speckle Properties and Speckle Models

2.3.1 Speckle Formation

When a radar illuminates a surface that is rough on the scale of a radar wavelength, the return signal consists of waves reflected from many elementary scatterers within a resolution cell. The distance between the elementary scatterers and the receiver vary due to the surface roughness. Therefore, the received waves, although coherent in frequency, are no longer coherent in phase. If the waves add relatively constructively, a strong signal is received; otherwise a weak signal may be received due to destructive combination of out of phase waves. A SAR image is formed by coherently processing the returns from successive radar pulses. The result is pixel to pixel variation in intensity, and this variation manifests itself as a granular pattern, called speckle (see a typical example of a SAR image in Fig. 2.1). We see that a zone that is homogeneous on the ground can have a granular aspect in a SAR image with large variation in pixel intensities; moreover in heterogeneous re-

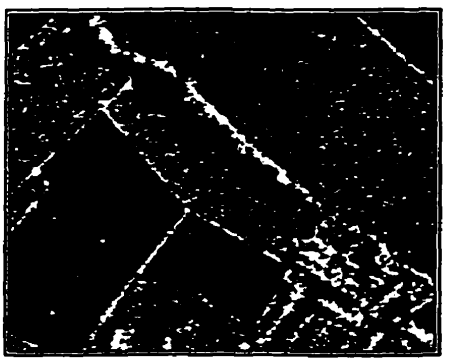

Figure 2.1: A typical SAR image.

gions of such an image, speckle noise can obscure image details by randomly modifying the pixel intensities. These effects may prohibit the abilities of human or computer vision systems to extract information from SAR images. Thus although speckle noise carries information about the microstructure of an imaged area, speckle is usually treated as noise in image processing applications.

2.3.2 Speckle Statistics for One-look and Multi-look SAR Images

A common approach to speckle reduction is to average several independent looks of the image. In SAR practice, this is accomplished by dividing the synthetic aperture length (or equivalently, the Doppler frequency spectrum) into N segments. Each segment is processed independently to form either an intensity or an amplitude SAR image, and the N images are summed together to generate an N-look SAR image. The averaging process corresponds to

the averaging of N independent samples. The N-look processing reduces the standard deviation of speckle. For intensity SAR images, the reduction factor is $\sqrt{N}$ while for amplitude SAR images, the reduction factor is N. However, this is accomplished at the expense of resolution which deteriorates by a factor of N in each spatial dimension.

SAR images formed without averaging are called one-look or single-look images. The Rayleigh speckle model serves as a good model for one-look amplitude SAR images [47]. For N-look amplitude SAR images, however, the speckle has a χ distribution with $2N$ degrees of freedom. Most commonly, four-look amplitude images are generated. In this case, the speckle has a much narrower distribution than the one-look amplitude Rayleigh distribution.

2.3.3 Speckle Models

The *multiplicative* nature of speckle noise has been verified by scatter plots of sample standard deviation versus sample mean produced in many homogeneous areas in SAR images [26]. Thus the multiplicative speckle noise model is mostly adopted in many SAR image processing algorithms:

$$y(i,j) = x(i,j) \cdot n(i,j) \tag{2.1}$$

where $y(i,j)$ is the (i,j)th intensity or amplitude of a SAR image pixel, $x(i,j)$ is the noise-free quantity at (i,j) and $n(i,j)$ is the speckle noise characterized by a distribution with a unity mean ($E[n] = 1$) and a standard deviation σ_v.

It can be easily verified that in featureless image regions,

$$\sigma_v = \frac{\sqrt{\text{var(y)}}}{E[y]} \tag{2.2}$$

is relatively constant as $E[y]$ changes. In other words, σ_v is the ratio of the variance to the mean. σ_v can be used as a measure of speckle strength.

Tur *et al* [46] argued against the validity of the multiplicative model of speckle noise, and proposed a model that takes into account the correlation of the speckle:

$$y(i,j) = [x(i,j) \cdot n(i,j)] * h(i,j) \tag{2.3}$$

where $h(i,j)$ is the point spread function of a SAR system and $*$ denotes the convolution operation. Some filters have been developed based on this multiplicative-convolutional model. But many speckle filters are designed using the simple multiplicative model. It should be mentioned that the multiplicative speckle model breaks down in the presence of some image features such as a point scatterer, lines, corner features, etc. But this simple model covers most images most of the time.

2.4 Speckle Noise Filters

Since speckle noise contaminates image content and thus detracts from image interpretation, speckle noise reduction is usually employed prior to further image analysis. The primary goal of speckle filtering is to reduce speckle noise without sacrificing information content. The ideal speckle filter should

adaptively smooth speckle noise, retain edges and features, and also preserve subtle but distinguishable details, such as thin linear features and point targets. Various speckle filters have been devised. However none of them can satisfy all of the requirements, and moreover, it is also difficult to determine which one is the best filter for speckle reduction due to their different processing purposes and their different capacities in handling different image content. Therefore, in this part we will not rank these filters according to the criteria which may favor some certain filters. We will only briefly describe some of the most popular techniques in order to give the reader an introduction to the different perspectives in this area. More detailed descriptions of these filters are best found in the specific references.

The mean filter

The mean filter is a simple averaging filter that replaces a center pixel of a sliding window by the mean value of the pixels in its neighbour window. This filter has a good noise smoothing capability, but this indiscriminate averaging causes a resolution loss, i.e, blurring in the vicinity of sharp edges.

The median filter

With a median filter and its variations the central pixel of a sliding window is replaced by the median intensity of all pixels within this window. Although this simple filter is effective in removing impulse or short duration noise, it is not well suited to speckle noise. Blurring of edges, erasing thin linear features

and object shape distortion are the common problems of this filter [37].

The Lee Multiplicative Filter

The Lee multiplicative filter[25] is designed to overcome the difficulties of indiscriminate averaging of the mean filter, and is based on the multiplicative speckle model, adopted and verified by Lee,

$$y(i,j) = x(i,j) \cdot n(i,j)$$

Lee assumed that the mean and variance of the noise-free original image x can be estimated from local mean and local variance of the observed image y. Thus,

$$\bar{y}(i,j) = \bar{x}(i,j) \cdot \bar{n}(i,j) \tag{2.4}$$

$$\text{var}(x) = \frac{\text{var}(y)(i,j) + \bar{y}^2(i,j)}{\sigma_v^2 + \bar{n}^2(i,j)} \tag{2.5}$$

where $\bar{y}$ and $\text{var}(y)(i,j)$ are approximated by the sliding window mean and variance, respectively, with the assumption that $\bar{n} = 1$. $E[(\hat{x} - x)^2]$ can be minimized to yield the estimated noise free image $\hat{x}$, i.e.,

$$\hat{x}(i,j) = \bar{x}(i,j) + k(i,j)[y(i,j) - \bar{x}(i,j)] \tag{2.6}$$

where

$$k(i,j) = \frac{\text{var}(x)(i,j)}{\bar{x}(i,j)\sigma_v^2 + \text{var}(x)(i,j)} \tag{2.7}$$

This implies that in homogeneous areas, the local variance is close to 0, thus the filtered pixel is set to the average of pixels in the window. For

high contrast regions or edge areas where the local variance is usually larger. the pixel value is unchanged in order to preserve the feature. Although the assumption that $\bar{n}(i,j) = 1$ is made in this algorithm, this restriction is not severe since any other value of $\bar{n}$ can be factored into the equation above. The value of σ_v can be supplied by the user based on prior knowledge of the image or can be estimated from the image directly using Equ. 2.2. The Lee multiplicative filter can effectively reduce speckle in homogeneous areas. However, a common characteristic of this filter is that the noise in the edge areas in not smoothed. This problem is reported to be eliminated by using an edge directed refined filter also proposed by Lee [27]. There have been many variations to this filter reported in literature with different degrees of improvements [5, 23, 24, 31]. As the Lee multiplicative filter is the most famous speckle filter, we will compare the performance of the proposed wavelet domain filter with this filter, using appropriate chosen parameters.

The Sigma filter

The Sigma filter[28] is based on the sigma probability of a Gaussian distribution. It filters the image noise by averaging only those pixels within the two standrad deviation (2σ) range of the center pixel within a sliding window. Pixels outside the two sigma range are considered as outliers and ignored. Thus, the estimated pixel intensity $\hat{x}(i,j)$ can be expressed as

$$\hat{x}(i,j) = \frac{1}{N_e} \sum_{k=i-n}^{n+i} \sum_{l=j-m}^{m+j} \delta(k,l) \cdot y(k,l) \tag{2.8}$$

where $y(i,j)$ is the noise degraded image intensity. N_e is the total number of pixels summed, and $\delta(k,l)$ is defined as

$$\delta(k,l) = \begin{cases} 1 & \text{if } y(k,l) \text{ is within } 2\sigma \text{ of } y(i,j) \\ 0 & \text{otherwise} \end{cases} \tag{2.9}$$

Consequently, high contrast features are preserved. However, dark spot noise is not removed from the SAR image. This is due to the relatively small variation range associated with dark pixels corrupted by speckle noise, and as a result no filtering action is taken for such pixels.

The Frost filter

Frost *et al* [17] proposed a spatial domain adaptive Wiener filter using a $(n \times n)$ sliding window. Like the Lee Multiplicative filter and the Sigma filter, it is also based on the multiplicative model. The Frost filter assumes that the useful information has an exponential autocorrelation function, i.e., that the image is stationary in a significant neighborhood of the filtered pixel. In this case, the estimate of the image can be obtained by

$$\hat{x}(i,j) = y(i,j) * f(i,j) \tag{2.10}$$

where $f(i,j)$ denotes the impulse response of the filter, and can be represented by

$$f(i,j) = k \cdot \alpha_f(i,j) \cdot \exp(-\alpha_f(i,j)\sqrt{i^2+j^2}) \tag{2.11}$$

where k is a normalizing constant, α_f is the decay constant which depends on the local statistics of the image

$$\alpha_f(i,j) = \frac{4\,\sigma_x^2\,(i,j)}{L\,\sigma_v^2\,\bar{x}^2(i,j)} \tag{2.12}$$

where $\bar{x}$, σ_x^2 are the local mean and local standard deviation of the image. σ_v^2 is the noise standard deviation, and L is the number of looks used in forming this image. Therefore, the pixel value at (i,j) is replaced by a weighted sum of the sliding window centered on this pixel with weights exponentially decreasing with the distance. In addition, the relative weights are controlled according to the window homogeneity. In uniform regions (small variance) or brighter regions (high mean), the speckle noise may appear more prominent, and hence the weights are more evenly distributed than they are in darker or heterogeneous regions. Compared with the Lee multiplicative filter, the Frost filter does more averaging in the edge areas, thus the noise in the edge areas is less prominent than with the Lee multiplicative filter, but the edges are somewhat blurred.

Other Filters Other spatial domain speckle filters include the geometrical filter [12], the morphological filter [41], the 2-D block Kalman filter [6] and the rational filter [38]. There are other approaches to speckle noise reduction. Some researchers tried the wavelet transform domain median filter and reported good results[8]. Another group used oversampled wavelet representations of SAR images to detect edge pixels and smooth noise [18]. The

research at Rice University is quite active in this area; Odegard *et al* reported the wavelet coefficient soft-thresholding approach to speckle suppression[36]. This approach will be detailed in the next chapter.

Summary

In this chapter, we have reviewed topics concerning SAR imaging systems and speckle noise. Speckle corruption is an important characteristic of SAR images and must be taken into account in SAR image processing and applications. In subsequent chapters of the thesis, we will present a new speckle smoothing method to enhance the compressibility of SAR images. The proposed method is based on the simplified multiplicative speckle model. Test results obtained from the proposed filter, compared with those of the Lee multiplicative filter, are found in Chapter 5 and Chapter 7.

Chapter 3

Wavelet Transform and Applications

The wavelet transform is emerging as an important mathematical representation. It is the combination of a nice theoretical foundation and many promising applications. It has particular abilities in handling non-stationary signals by offering good localization in both the spatial and frequency domains. The wavelet transform can find applications in many areas. In this thesis, we use it as an image processing and compression tool to accomplish noise smoothing and image compression tasks simultaneously.

In this chapter, we repeat some basic theory of wavelets, as required for further use in this thesis. We begin with one-dimensional signals for notational simplicity, and then extend our discussion to two-dimensional image signals realized in a separable way. For a more comprehensive overview, the reader is referred to [14, 32, 48]. As the second part of literature review, this chapter also outlines several image compression algorithms, especially those

reported for SAR image compression.

3.1 Introduction to Wavelet Transform

Wavelets are functions of a real variable generated from one single function, the *mother wavelet* ψ by dilations and translations.

$$\psi_{a,b}(x) = |a|^{-1/2}\psi(\frac{x-b}{a}) \qquad a, b \in R, \quad a \neq 0 \tag{3.1}$$

where a and b are parameters of dilation and translation, respectively. Here, we assume $x \in R$ is a one-dimensional variable. The mother wavelet ψ has to satisfy the following admissibility condition.

$$\int_{\infty}^{\infty} \frac{|\Psi(\omega)|^2}{|\omega|} d\omega < \infty \tag{3.2}$$

where Ψ denotes the Fourier transform of ψ. Moreover, if ψ has sufficient decay, then Equ.(3.2) is equivalent to

$$\int_{-\infty}^{+\infty} \psi(x)dx = 0 \tag{3.3}$$

which means that the wavelet ψ exhibits at least a few oscillations. There is a large choice of possible functions ψ, such as the Meyer wavelets, the Battle-Lemarie wavelets, the Haar wavelets and the Daubechies wavelets [14]. These wavelets can be chosen for different applications. Among these, the Daubechies wavelets are especially useful for signal/image processing purposes because wavelets belonging to this category have finite support and thus they can be implemented using finite impulse response filters.

The idea of the wavelet transform is to represent any arbitrary function f as a superposition of wavelets. This function f can then be decomposed at different scales or resolution levels. One way to achieve such a decomposition involves writing f as an integral of $\psi_{a,b}$ over the parameters a and b using appropriate weighting coefficients. In practice, however, it is preferable to express f as a discrete sum rather than as an integral. The coefficients a and b are thus discretized such that: $a = a_0^m$ and $b = nb_0a_0^m$ with $m, n \in Z$ where $a_0 > 1$, $b_0 > 0$ are fixed. The wavelet is then defined as follows:

$$\psi_{m,n}(x) = \psi_{a_0^m, nb_0a_0^m}(x) = a_0^{-m/2}\psi(a_0^{-m}x - nb_0) \tag{3.4}$$

and the wavelet decomposition of f becomes

$$f = \sum_{m,n} c_{m,n}(f)\psi_{m,n} \tag{3.5}$$

where $c_{m,n}(f)$ is given by

$$c_{m,n} = < f, \psi_{m,n} > \tag{3.6}$$

Depending on the scaling parameter a, the wavelet function $\psi_{m,n}$ dilates or contracts in time, causing the corresponding contraction or dilation in the frequency domain. For large, positive values of m ($a > 1$), the $\psi_{m,n}$ function is highly dilated and hence large values for the translation step b are well adapted to this dilation. This corresponds to low frequency or narrow-band wavelets. For large negative values of m ($a < 1$), the $\psi_{m,n}$ function is highly concentrated and the translation step b should take small values. These

functions correspond to high frequency or wide-band wavelets. Therefore, the wavelet transform achieves a "flexible" time–frequency resolution. As a result, wavelets are better suited for representing both short bursts of high frequency and long duration slowly varying signals.

3.2 Wavelet Transform and Multiresolution

The concept of multiresolution analysis introduced by S. Mallat [32] is a mathematical tool particularly well adapted to the use of wavelet bases in image analysis.

We first focus on the algorithm for one-dimensional signals. In addition to the wavelet function ψ, another function ϕ, which is called a scaling function, is introduced. This ϕ is in fact a low-pass filter that complements the wavelet functions in representing a signal at the same scale. For notational simplicity, the wavelet coefficients $c_{m,n}(f)$ will be written as $c_m(n)$ since we are working with sampled signal $s_m(n)$.

Let $s_0(n) \in l^2(Z)$ be a sampled signal to be decomposed into several resolution levels corresponding to different spatial-frequency bands. Let $h(n)$ and $g(n)$ be associated with the wavelet and scaling function by

$$\phi(t) = 2\sum_n h(n)\phi(2t-n) \tag{3.7}$$

$$\psi(t) = 2\sum_n g(n)\phi(2t-n) \tag{3.8}$$

where $h(n)$ and $g(n)$ satisfy

$$\sum_n h(n) = \sqrt{2} \tag{3.9}$$

$$\sum_n g(n) = 0 \tag{3.10}$$

and are related by

$$g(n) = (-1)^n h(-n+1) \tag{3.11}$$

Thus, this decomposition can be achieved using

$$s_m(n) = \sum_k h(2n-k) s_{m-1}(k) \tag{3.12}$$

$$c_m(n) = \sum_k g(2n-k) s_{m-1}(k) \tag{3.13}$$

Since $h(n)$ and $g(n)$ are associated with an orthogonal wavelet basis, they ensure the exact reconstruction of the signal $s_{m-1}(n)$. The reconstruction formula is as follows:

$$s_{m-1}(k) = \sum_n h(2n-k) s_m(n) + \sum_n g(2n-k) c_m(n) \tag{3.14}$$

The signal $s_m(n)$ is an approximation of signal $s_{m-1}(n)$ at resolution 2^{-m}. The wavelet coefficients $c_m(n)$ represent the information lost when going from an approximation of the signal s with resolution 2^{-m+1} to a coarser approximation of s with a resolution 2^m. According to Shannon's theorem, these signals can be undersampled by a factor 2.

The implementation of multiresolution analysis involves decomposing a signal $s_0(n)$ into two "subsignals" $s_1(n)$ and $c_1(n)$. This operation can be

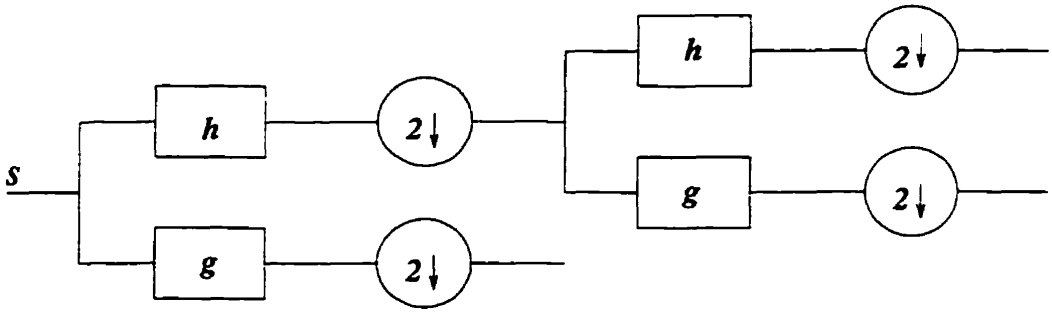

Figure 3.1: Dyadic wavelet transform of a signal s

repeated on signal $s_1(n)$ and so on up to resolution 2^{-J}(Fig. 3.1). In this case, the signal set $c_1 \cup c_2 \cup c_3 \cup \ldots \cup c_i \cup c_j \cup s_j$ provides a lossless representation of s_0, and hence enables the exact reconstruction of this signal. This orthogonal multiresolution analysis is characteristized by a resolution factor of 2 between two consecutive scale levels, and is thus called *dyadic* multiresolution analysis.

In the above discussion, we used an orthogonal wavelet basis. However, such a basis is impractical in image processing because the associated filters have nonlinear phase. Since there is no orthogonal linear phase FIR filters enabling exact reconstruction, the orthonormality constraint has to be relaxed by using *biorthogonal bases* [11]. It is worth noting that the development of the biorthogonal wavelet theory is of key interest for image coding because it enables the definition of different filter banks for analysis and synthesis. As in the orthonormal case, we associate the wavelet basis function and the scaling function with the filter bank $h(n)$ and $g(n)$. But we need two other filters $\tilde{h}(n)$ and $\tilde{g}(n)$ to deal with the biorthogonal basis. The following relationship

must hold between them:

$$\tilde{g}(n) = (-1)^n h(-n+1) \tag{3.15}$$

$$g(n) = (-1)^n \tilde{h}(-n+1) \tag{3.16}$$

and

$$\sum_n h(n)\tilde{h}(n+2k) = \delta_{k,0} \tag{3.17}$$

The decomposition (analysis) algorithm and the reconstruction (synthesis) algorithm have the same structure as the orthonormal case. The decomposition algorithm is unchanged, and the reconstruction is expressed as

$$s_{m-1}(k) = \sum_n \tilde{h}(2n-k)s_m(n) + \sum_n \tilde{g}(2n-k)c_m(n) \tag{3.18}$$

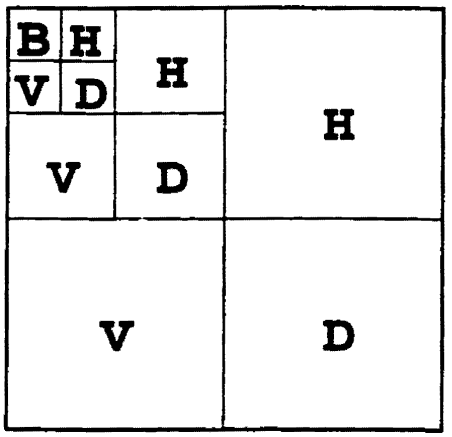

Figure 3.2: Schematic illustration of a three level wavelet decomposition of an image.

The above discussion can be easily extended to handle two-dimensional image signals. In practice, images to be processed are sampled signals. We

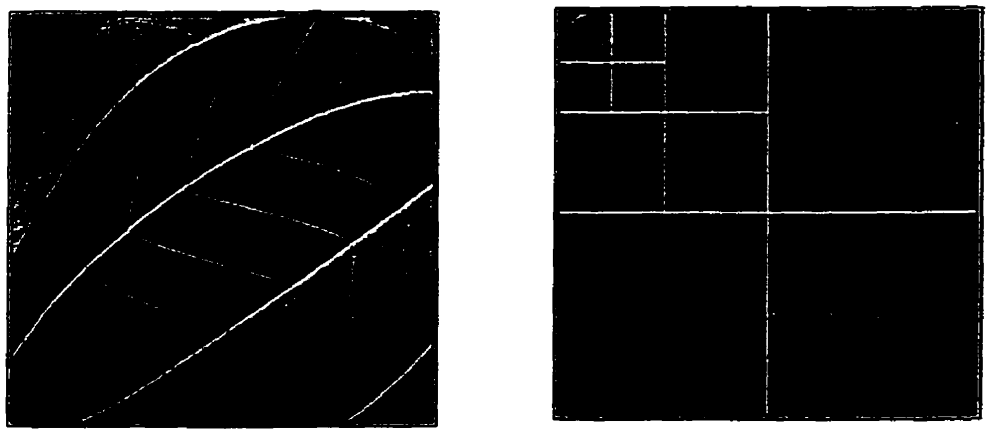

(a) (b)

Figure 3.3: Three level wavelet decomposition of an image. (a) Original *balloon* image. (b) Three level decomposition of (a).

call the original image at resolution 2^0. $s_0(n_x, n_y)$. Computation of the image $s_m(n_x, n_y)$ at lower resolution 2^{-m} and determination of the wavelet coefficients $c_m^d(n_x, n_y)$ which are interpreted as three inter-scale images can be achieved by convolution operations using separable two-dimensional filters. Filtering is applied independently on the image rows and columns. For a given resolution level M, the original image can be represented as a set of $3M + 1$ subimages (Fig. 3.2 and Fig. 3.3)

$$\{s_m\} \cup \{(c_m^H)_{1 \le m \le M}\} \cup \{(c_m^V)_{1 \le m \le M}\} \cup \{(c_m^D)_{1 \le m \le M}\} \tag{3.19}$$

and this set of subimages is the dyadic two-dimensional wavelet representation of the original image. Because of subsampling, the total number of pixels of this set of subimages is the same as the initial image. This separable multiresolution analysis method enables us to distinguish the horizontal

(c_m^H), vertical (c_m^V) and diagonal (c_m^D) features of the image.

3.3 Image Compression Using Wavelet Transforms

3.3.1 Overview

The concentration of image energy is one characteristic of the wavelet transform. The distribution of the wavelet coefficients can be well approximated by the Gamma function which is highly peaked at zero. This implies that the values of many coefficients are close to zero, and thus enables an image to be represented by only a few significant coefficients. Another important property is that the wavelet transform decomposes an image into different resolutions. Therefore, different bit allocation schemes can be applied to these coefficients according to their relative importance in image representation or possibly to the response of the human vision system.

The application of wavelet transforms in image compression has been well investigated. Various algorithms have been proposed to cope with different image compression problems. These algorithms differ in the following perspectives:

- **quantization strategy:** Scalar quantization and vector quantization are two general categories of quantization. Scalar quantization performs quantization on each individual coefficient, while vector quantization processes a group of coefficients at the same time. Usually

vector quantization can achieve higher information compaction at the expense of algorithm complexity and computational cost at the encoder. Scalar quantization is often exploited in wavelet based compression algorithms. The Efficient Pyramid Image Coder (EPIC) outlined later in this section uses scalar quantization. Another algorithm which is also outlined later. the Embedded Zerotree Wavelet (EZW) coding algorithm, uses an implicit scalar quantization scheme.

- **entropy coding method:** Run length coding and Huffman coding are usually exploited to encode the quantized coefficients. Arithmetic coding is another entropy coding approach which can achieve better compression, but the algorithm itself is more complicated.

- **choice of filter banks:** Antonini *et al* [4] suggested that the regularity or differentiability, which describes how many times a wavelet can be differentiable, is an important measure and recommended using a filter bank with higher regularity in designing compression algorithms. But further studies by Villasenor *et al* [49] suggested that regularity is not the only measure of the filter banks, nor to say the best measure. They found that the most common and objectionable artifact in reconstructed images is ringing near sharply defined features. To suppress ringing effect, filters with favorable peak to sidelobe ratio or with low undershoot of the second oscillation are preferred. They evaluate over 4300 candidate filter banks, and concluded the Daubechies 9/7 wavelet

is "good overall". This conclusion is coincidently identical with that obtained from regularity measure consideration; moreover this filter bank has been intuitively selected in many image compression algorithms.

In the remainder of this section, two wavelet based compression algorithms are outlined, namely the Efficient Pyramidal Image Coder (EPIC) and the Embedded Zetotree Wavelet Coder (EZW). Their performance on SAR image compression will be evaluated in Chapter 4. The EZW algorithm is also adopted in the multi-rate compression scheme presented in Chapter 6.

3.3.2 Efficient Pyramid Image Coder (EPIC)

The EPIC [2] is an experimental image data compression algorithm designed by Edward H Adelson and Eero P Simoncelli. The compression algorithm is based on a bi-orthogonal critically-sampled dyadic wavelet decomposition and a combined run-length/Huffman entropy coder. The filters have been designed to allow extremely fast decoding on conventional (i.e. non-floating point) hardware, at the expense of slower encoding and a slight degradation in compression quality (as compared to a good orthogonal wavelet decomposition). Because a wavelet transform is used instead of the Discrete Cosine Transform (DCT), blocking effects are alleviated.

As an experimental compression algorithm, quantization bin sizes in this algorithm are chosen to be the same for each subband, and a very simple

scalar entropy coding scheme is adopted to compress the quantized subbands.

After the quantization, run length coding is employed to encode the quantized wavelet coefficients. Coefficients with continuous zero quantization value along the scan line are grouped together and the length of the zero runs can be encoded efficiently. The position and the value of the nonzero coefficients are encoded with more bits.

3.3.3 Embedded Zerotree Wavelet Coefficient Compression Algorithm

The EZW is another wavelet based compression algorithm designed by J. Shapiro [44]. In this algorithm, every coefficient (a parent) in a given scale except the finest scale is associated with a set of coefficients (children) at finer scales of a similar orientation. Shapiro assumed that given a threshold, if a parent coefficient is below this threshold (insignificant), its children are very likely to be insignificant too. He then divided coefficients into *significant*, *zerotree* and *isolated zerotree*. Coefficients whose values are above a threshold are *significant* in their information content and therefore need to be encoded with high fidelity. If a parent is insignificant and all its children are insignificant too, this set of coefficients is called a *zerotree*. If a parent is insignificant, but at least one of its children is significant, this set of coefficients is called an *isolated zerotree*. Because there can be a large percentage of coefficients which are "small" in the decomposition of an image, if the absence of significance can be well predicted, only the positions of zerotree

parents need to be encoded in order to represent the large amount of insignificant coefficients; and hence more bit budget can be allotted to encode the significant and isolated zerotree coefficients.

EZW algorithms have some other features. In EZW, wavelet coefficients are re-ordered such that bigger coefficients are encoded first. This is to ensure that more important information is transmitted with higher priority. The detected significant wavelet coefficients are successively approximated with the most significant bit of these coefficients transmitted first followed by less significant bits. This provides a compact multi-precision representation of the significant coefficients and facilitates the embedded coding algorithm. The performance is further enhanced by using the adaptive arithmetic coding.

S. Said and W.A. Pearlman improved the original EZW algorithm based on set partition [42] of wavelet coefficients. The improved algorithm has a similar structure as EZW, but has a slightly better performance. This algorithm will be outlined in Chapter 6 and adopted in the multi-rate compression scheme.

3.4 Image Processing in the Wavelet Domain

3.4.1 Overview

There are several reasons for using wavelet transforms for image processing purposes:

- good spatial-frequency resolution;

- multiresolution notation;
- link with digital filter banks;
- fast implementation algorithms;
- linear phase property for bi-orthogonal wavelet families.

The multiresolution representation of a wavelet transform provides a natural way to approach adaptive processing. Unlike many spatial domain image processing techniques which lack capabilities for treating large and small scale image content adaptively, the multiresolution property of the wavelet transform offers a means of handling both large and small scale image content separately and flexibly. The choice of sliding window size in many spatial domain median filters is a factor compromising noise reduction and structure preservation. In the wavelet transform domain, this issue can be handled with more flexibility. For example, a size-decreasing median filter in the wavelet domain has been designed by Boroczky *et al* [8]. At any level, because the noise energy of a certain decomposition level is decreased and the amount of structure information tends to increase relative to the previous level, they decreased the window size of the median filter accordingly and obtained good results.

The basis functions used in the wavelet transform are locally supported. Thus, sharp transitions (i.e. edges) in images are non-zero only over a short duration in the wavelet domain, i.e., they do not propagate to other far-

neighbor coefficients as they do in the Fourier transform. Therefore, the processing of the coefficients can be performed locally without influencing other coefficients. This locally supported property also distinguishes the wavelet transform from many spatial domain sliding window approaches which process pixels on a group basis; hence the wavelet approaches can consequently avoid the blurring of edges.

The wavelet transform has been used effectively in many image processing applications, such as image enhancement, texture classification or segmentation and object recognition. In the next part of this section, we briefly outline the wavelet coefficient soft-thresholding method which has found applications in noise reduction.

3.4.2 Wavelet Coefficient Soft-thresholding Method

Soft-thresholding was proposed by Donoho [16] as a nonlinear technique for reconstructing an unknown function from noisy data. It attempts to reject noise by damping or thresholding in the wavelet domain.

Suppose we wish to recover an unknown finite length function x from noisy data y, i.e.

$$y_i = x_i + n_i, \qquad i = 0, 1, \cdots, N-1 \tag{3.20}$$

where x_i is the true signal, and n_i is white Gaussian noise with variance σ. Let $\hat{x}$ be the estimate of x.

Our goal is to optimize the mean-square error

$$\frac{1}{N} E\,||\hat{x} - x||_2^2 = \frac{1}{N} \sum_{i=0}^{N-1} E(\hat{x}_i - x_i)^2 \tag{3.21}$$

subject to the side condition that with high probability, $\hat{x}$ is at least as smooth as x. The soft-thresholding method has three steps:

1. Apply the wavelet transform to the measured data y_i, obtaining the wavelet coefficients v_i.

2. Compute the threshold $t = \sigma\sqrt{2\log(N)}$.

3. Apply soft-thresholding,

$$\eta_t(v_i) = \begin{cases} v_i - t & v_i > t \\ 0 & -t \le v_i \le t \\ v_i + t & v_i < t \end{cases}$$

4. Apply the inverse wavelet transform, recovering $\hat{x}_i$, $i = 0, 1, \cdots, N-1$.

A detailed description of this method can be found in [16].

It has been shown that this method has three distinct features: 1) The estimate $\hat{x}$ achieves almost the minmax mean square error over a wide range of smoothness classes, including many classes where traditional linear estimators do not achieve; 2) This procedure maintains the sharp features of x (i.e., the edges in images), and therefore provides better visual quality than procedures based on mean-squared error alone; 3) The estimate does not exhibit any noise-induced structures, unlike most minimum mean square methods.

The only parameter in this method is the threshold. The universal threshold $t = \sigma\sqrt{2\log(N)}$ was designed for the purpose for suppressing noise-induced spikes which spoil the smoothness of reconstructions. However, if we only want to minimize the mean-square-error, we can choose other thresholds.

Applications of this technique have been reported in [19, 36] with promising results. However, while speckle noise is reduced by soft-thresholding, the indiscriminate processing of every wavelet coefficient usually modifies the intensity of the edge pixels as well as the noisy ones in homogeneous regions and gives the filtered image a blurred and dimmed appearance.

To overcome this problem, in Chapter 5 we make use of the intra- and inter-band correlation among wavelet coefficients to distinguish edge pixels from noise. Only those coefficients that are not classified as edge are processed by soft-thresholding and thus the prominent edge pixels are better preserved.

3.5 Image Compression Methods for Remote Sensing Images

Recent years have seen a tremendous increase in the generation, transmission, and storage of remotely sensed images. Although much work has been done towards developing algorithms for compressing optical image data, techniques that exploit the special nature of SAR and other remote sensing images have

only started to emerge recently. In this section, image data compression techniques used in SAR and other remote sensing applications will be briefly reviewed.

As mentioned previously, compression schemes can be broadly classified into two categories; *lossy* compression and *lossless* compression. Lossless compression may be required for data archiving and other situations where the pixel values are used to compute other indicators of interests such as vegetation index or in other applications where high detail is a requirement. Lossless compression techniques typically provide compression ratios of up to 2 or 3 [43]. Lossy compression is usually used for image dissemination purposes where larger amount of information loss may actually be preferable to reduce the transmission delay. Much larger compression ratios can be achieved by lossy compression of SAR images.

3.5.1 Lossless Compression

The goal of lossless image compression is to represent a given image with a minimum number of bits. This is generally achieved in two steps. First, statistical redundancy in the image is removed and a *residue* image is obtained. This is called *decorrelation*. In the second step, the residual image is encoded into a binary string using entropy coders. This is the *coding* step. Most of the compression is normally attained in the decorrelation steps. Lossless predictive coding algorithms are most commonly used. In predictive coding, a combination of neighboring pixel values are used to predict the value of the

pixel being encoded. The prediction error is then encoded. This technique makes use of the correlation within images. For a single band image, only spatial redundancy within an image can be exploited while for multispectral images, increases in compression ratios can be obtained by removing spectral redundancy in addition to spatial redundancy. Successful lossless compression algorithms have been reported in [43, 51].

3.5.2 Lossy Compression

Lossy compression techniques achieve higher compression ratios at the expense of information loss. Lossy predictive coding, transform coding, vector quantization and subband/wavelet compression are examples of this category. As lossy compression is the focus of this thesis, we will discuss these techniques in more details.

Lossy Predictive Coding

As in lossless predictive coding, a pixel value being encoded is predicted from a combination of neighbouring pixel values, and only the prediction error is encoded. The lossy approach achieves more compression by using slightly poorer approximations of the prediction error. But still only a limited degree of compression can be achieved by this technique [10].

Transform Coding

The idea behind transform coding is to decorrelate the image pixels and concentrate the energy of an image onto only a few transform coefficients. The most commonly used transform is the discrete cosine transform (DCT). and the current standard of still image compression algorithm JPEG [50] belongs to this category. The major drawback of this technique is its apparent blocking effect in the reconstructed image due to the infinite duration of the sinusoidal basis function used in the DCT. This technique is also evaluated in [10]. We will further evaluate the JPEG algorithm for SAR image compression in Chapter 4.

Subband/Wavelet Transform Coding

Subband coding is based on dividing an image into its spatial frequency bands, then quantizing the coefficients describing the band images according to their relative importance. The wavelet transform can be considered as a special case of subband coding where the filter used in subband coding should satisfy some characteristics [4]. As already noted above in Section 3.3.2, the wavelet based methods can avoid the blocking effect problem since the support of the base functions can be compact [1]. More discussion about the wavelet transform will be addressed in the following chapters.

Vector Quantization

Vector quantization (VQ) [22] is a compression technique in which an image is divided into groups of pixels and then matching is performed in order to find a vector in a predefined codebook which is closest to this group of pixels. Only the label of the vector in the codebook is encoded and transmitted. Encoding with VQ is computationally expensive at the encoder since obtaining the codebook is also part of VQ work, but the decoding procedure is very efficient as it can be implemented as a a table look-up. VQ is very attractive for image distribution applications because of its asymmetric characteristics at encoder and decoder. But it also has several disadvantages, such as large encoding complexity, strong scene dependence, and severe edge degradation. This evaluation of VQ techniques for SAR image compression applications is also reported in [10].

There are other data compression techniques for remote sensing image applications, such as fractal based image compression [7] and segmentation based image compression [54]. All these techniques lead to some degree of data reduction and provide more viable and efficient collection and distribution of information.

Summary

In the chapter, we have reviewed the wavelet transform and its applications in image compression and processing. In particular, two wavelet transform based compression algorithms. EPIC and EZW, and the wavelet coefficient soft-thresholding technique are described. The following chapters present our work with SAR image compression using these methods. We begin with the evaluation of conventional compression algorithms to study the effect of speckle noise in SAR images on image compression. Then we refine the soft-thresholding method to smooth speckle noise. We implement a multi-rate compression scheme based on the EZW algorithm to handle large size SAR images with a variety of image content.

Chapter 4

Evaluation of Image Compression Methods for SAR Images

4.1 Introduction

As we discussed in Chapter 1, for many archiving purposes it is desirable that we compress SAR images without any loss of information. But there are many other situations where lossy compression is preferred. Compared with lossless compression, lossy compression for SAR images has not been fully investigated. In this chapter, we will report our experience with SAR image compression using three lossy compression methods which have been successfully used for optical image compression. The purpose of this preliminary research is to reveal experimentally the difficulties of SAR image compression, and thus formulate our compression approach. Two wavelet based image compression algorithms, EPIC and EZW, are evaluated. The

Joint Picture Encoding Group (JPEG) algorithm is also included in our evaluation for comparison. We begin with a description of the test data set selected for use throughout the study.

4.2 Test Data Set

We use both airborne SAR images and simulated speckled images in our evaluations. The real SAR image data was collected by the Canadian Center of Remote Sensing (CCRS). The original SAR data set was converted to real amplitude SAR images and then focused in order to obtain approximately square image pixels (roughly a 4-look averaging process in amplitude) [52]. The simulated images are created by the MATLAB image processing toolbox [45].

In obtaining the real SAR image data, the CCRS airborne SAR was flown over a region near Ottawa; Thus the images contain a variety of scene content. Several typical sub-images were extracted from the processed image data set and two of them are used in the evaluation. One is an area of countryside with fields and forest. We consider it as an easy image because it contains relatively simple image contents (mainly road and fields). We call this extraction *ext1* (see Fig. 4.1-(a)). The other one is an area consisting of an industrial suburb. This image contains some large homogeneous areas, but there are also many man-made objects which have more details. We call this image *industry* (Fig. 4.1-(b)). These two extractions represent typical

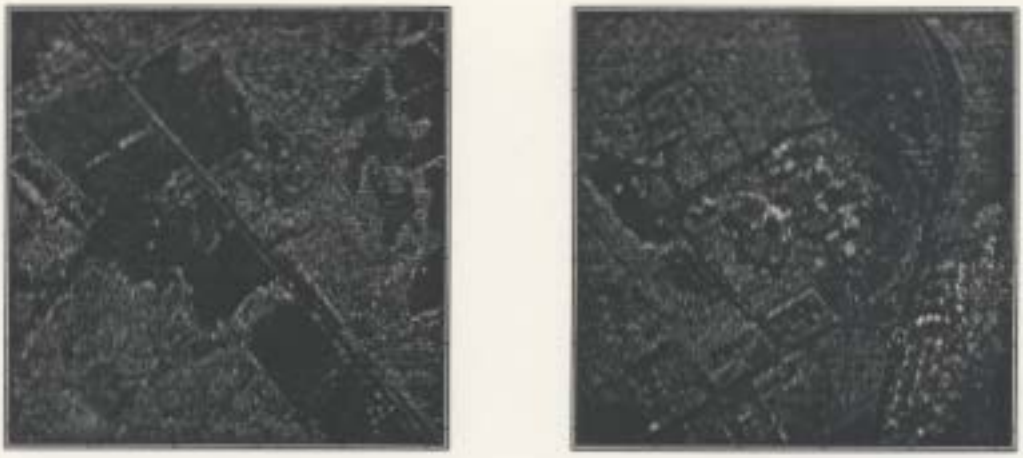

(a) (b)

Figure 4.1: Two SAR image extractions used in the evaluations: (a) *ext1*; (b) *industry*.

scene content and have been used in the development and testing of many other image processing algorithms [20, 23, 34].

In addition to the real SAR images, we also generated several simulated speckled images. The simple multiplicative speckle model is adopted in image generation. The speckle noise levels in the simulated speckled images are adjusted to be close to those measured in the real SAR images in homogeneous areas. The ratio of local variance to local mean in homogeneous areas is used as the speckle measure. For 4-look amplitude SAR images, this measure is approximately 0.26 [26]. Several simulated speckled images are generated and two of them will be used in the following evaluation. They are *airfield* (Fig. 4.2-(a)) and *stripe* (Fig. 4.2-(b)). The performances of the three compression algorithms on two well-known optical images *lena* (Fig. 4.3-(a))

(a) (b)

Figure 4.2: Two simulated speckled images used in the evaluations: (a) *airfield*; (b) *stripe*.

(a) (b)

Figure 4.3: Two optical images used in the evaluations: (a) *lena*; (b) *barb* (extraction).

and *barb* (Fig. 4.3-(b)) are provided for comparisons. All images used in our evaluations are of size 256 × 256 pixels. The external storage type of these images is one byte/pixel. However, they are stored and processed as floating point in our proposed methods.

4.3 Evaluation Criterion

We evaluate the overall compression performance using the standard bit-per-pixel (bpp) vs. Peak Signal to Noise ratio (PSNR) and peak error. Although it is still argued whether PSNR is a suitable measure for reconstructed image quality, it is used here because it provides a straightforward means for quantitative comparison. Since SAR images are usually processed automatically, it is critical that the reconstruction error of any pixels not exceed a given acceptable threshold. Thus, we include peak error as another measure in our evaluation.

In order to highlight the differences between optical and speckled image compression, we introduce several other measures which are related to the specific compression algorithms.

Measure for EPIC:

In EPIC as in many other transform based compression algorithms, run length coding is often exploited to encode the quantized transform coefficients. Since the run length coding scheme is intended to take advantage of the many zero coefficients in the wavelet domain, a run length distribu-

tion highly peaked at zero will correspond to a possible high compression ratio. If the same quantization strategy is used for all the images, the differences in run length distribution of the zero coefficients will reflect the final compression performance.

Measures for EZW:

The number of isolated zerotrees (IZs) will be used as a measure of EZW. As we described previously, an IZ is introduced when the across scale prediction of insignificance of wavelet coefficients is incorrect. Thus more bit budget is needed to encode the significance map. For an image without many details, the number of IZs can be expected to be small. In addition, *pages* and *times* are two other measures for EZW: *pages* counts the number of detected significant coefficients and *times* depicts how accurately these significant coefficients are successively approximated. Thus for a given bit-per-pixel rate, a smaller IZ value, together with a smaller *pages* value and a larger *times* value corresponds to better reconstruction quality.

4.4 Evaluation Results and Analysis

Fig. 4.4, 4.5 and 4.6 provide a graphical illustration of the compression performance of these three algorithms. Table 4.1, 4.3 and 4.2 show the results using these algorithms with some specific parameters. For EPIC, all images are 4-level decomposed and a bin size=20 is used to quantize the finest scale coefficients. For JPEG, the quality parameter is chosen such that

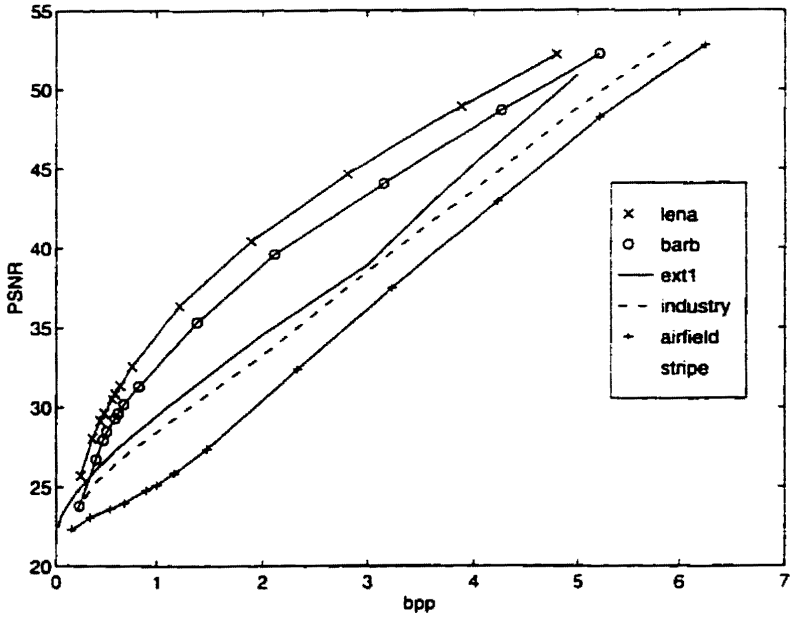

Figure 4.4: Compression using the EPIC algorithm

the reconstruction image quality is approximately 65% of the original one. A moderate bit-per-pixel rate bpp=1.5 is used for EZW. We also use these parameters in the comparisons of the EPIC and EZW measures.

For the EPIC algorithm with the fixed parameters, we see that the optical images are more compressible than both the simulated and real speckle images. In other words, these optical images can be represented as well as the speckled images but with smaller bit-per-pixel rates. The reconstruction errors in the EPIC algorithm are introduced mainly by quantization. Since we use the same quantization strategy for all these images, the peak errors for them are on the same level.

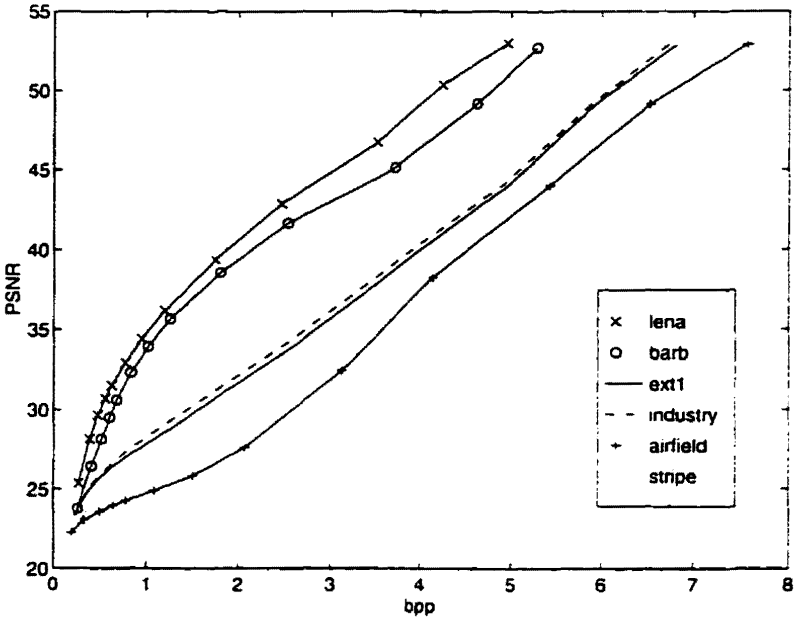

Figure 4.5: Compression using the JPEG algorithm

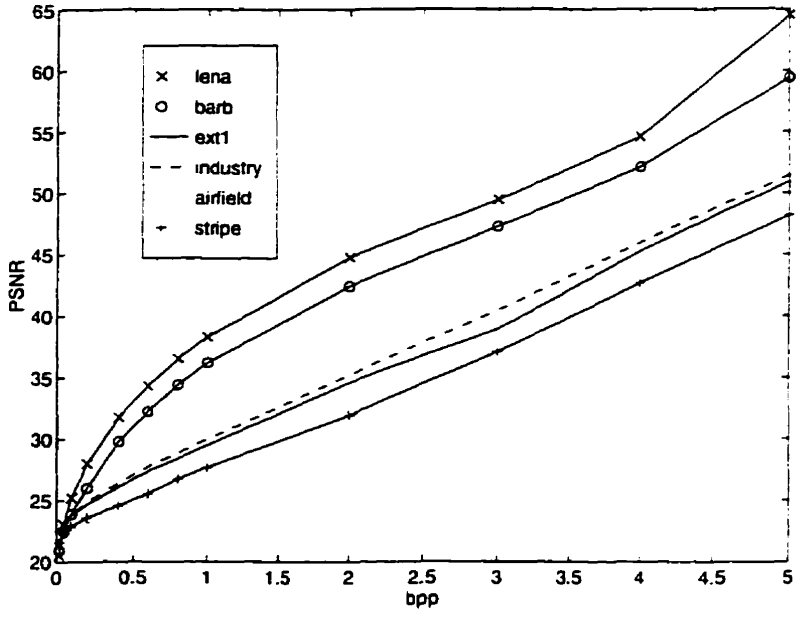

Figure 4.6: Compression using the EZW algorithm

Table 4.1: EPIC algorithm: decomposition level=4, bin size=20

image	lena	barb	ext1	industry	airfield	stripe
bpp	1.06	1.19	1.77	1.72	2.05	1.84
PSNR	35.14	33.96	31.65	31.86	30.83	30.84
peak	27	28	28	28	30	30

Table 4.2: Comparison results using JPEG algorithm: quality=65%

image	lena	barb	ext1	industry	airfield	stripe
bpp	1.14	1.20	1.65	1.62	1.94	1.74
PSNR	35.77	35.28	30.32	30.70	27.14	28.06
peak	31	31	45	47	57	59

Table 4.3: Comparison results using EZW algorithm: bpp=1.5

image	lena	barb	ext1	industry	airfield	stripe
PSNR	41.92	39.83	32.09	32.58	27.88	29.81
peak	14	13	31	35	47	43

For JPEG, similar results are obtained as those for EPIC. Again, the optical images are reconstructed with better quality. The differences in peak error is due to the quantization table used in JPEG, which is designed for the efficient compression of natural photographic images. As the characteristics of the real and simulated speckled images are quite different from those of optical images, the performance of JPEG is deteriorated.

The difference in the reconstructed image quality from the EZW algorithm is quite significant. Given a bit-per-pixel rate, we find the speckled images are reconstructed much more poorly than the optical images. The errors are introduced by the successive approximation, an implicit quantization strategy used in EZW, where some of the less significant bits of the coefficients are not encoded when the bpp is small. Since in EZW the significant and non-significant coefficients are approximated with different accuracies, the reconstruction error is not evenly distributed across every coefficient. As a result, we can expect that images reconstructed from EZW may highlight the major structures in images and provide better visual qualities.

From Fig. 4.4, Fig. 4.5 and Fig. 4.6, we may observe a pattern that the simulated speckled images are even more difficult to compress than the

real SAR images. This is because that the mean values of these two images are higher than those of the SAR images. Therefore, the simulated images have higher variances than the real SAR images, and hence they are less compressible from an image compression point of view.

Now, we use the EPIC and EZW measures to show how speckle noise influences SAR image compression. Table 4.4 shows the run length distributions of these six images using EPIC. We find that there are many more short runs in the decomposed SAR and simulated speckled images than those in the decomposed optical images. It is obvious that even for the simulated speckled image *stripe* which only contains simple image content that the numbers of short runs are substantial. These short runs reflect the large variance of speckled images. They are caused by speckle noise which may split potential long runs into many short runs.

Table 4.5 shows the EZW measures when these images are compressed using the EZW algorithm with bpp=1.5. We can see that there are more isolated zerotrees (IZs) in the decomposed speckled images than in the optical images. This is again the result of speckle noise because the constructive or destructive effect of speckle noise may weaken or totally destroy the across scale correlation. IZs are introduced when the across scale prediction of the coefficients' insignificance is incorrect. For bpp=1.5, we find the number of detected significant coefficients are quite similar for these images. Thus the EZW algorithm spends more bit budget to encode the significance

Table 4.4: Comparison of Run-length Distributions of Test Images Using EPIC (level=4, bin=20).

run length	lena	barb	ext1	industry	airfield	stripe
0-10	2697	3008	8652	8007	10461	13733
11-20	405	414	666	735	958	319
21-30	177	180	232	229	33	27
31-40	89	103	127	111	1	6
41-50	55	164	36	61	1	6
51-60	70	48	18	27	0	0
61-70	29	43	4	12	0	0
71-80	21	29	3	3	0	0
81-90	23	18	0	1	0	0
91-100	31	7	0	0	0	0
>100	169	119	0	2	0	0

map of speckled images which have more IZs. Accordingly, the informative coefficients will be scanned fewer times, resulting in poorer approximation accuracy. This explains the higher peak errors in the EZW reconstructed speckled images.

Table 4.5: Comparison of EZW performances with test images (bpp=1.5).

measure	lena	barb	ext1	industry	airfield	stripe
IZ number	6720	6193	8311	7777	9546	9545
pages	18	18	18	18	18	17
times	9	9	6	6	5	5

From the above evaluation, we understand that speckle noise contamination of SAR imagery is an important data characteristic that needs to be considered in designing a SAR image data compression algorithm. As a re-

sult of speckle noise, there is a weakened inter-pixel correlation among the adjacent resolution cells in the SAR images as compared to the optical images. Hence, image data compression techniques that are primarily based on inter-pixel correlation do not perform as effectively for SAR images. We find the inter-band correlation among coefficients is also weakened in speckled images, but the effect of speckle noise is comparatively less prominent with the EZW algorithm (see Fig.4.7). This conclusion suggests that we devise compression algorithms that basically exploit inter-band correlation. In the light of the above discussion, and due to other properties of the EZW algorithms, such as its embedded nature, we consider EZW to be one of the best candidates for future development in SAR image compression.

Moreover, because speckle noise is manifest as one obstacle to SAR image compression, we need to adopt a technique to remove or reduce speckle noise prior to SAR image compression. This will be the topic of the next chapter and the study of compression will resume in Chapter 6.

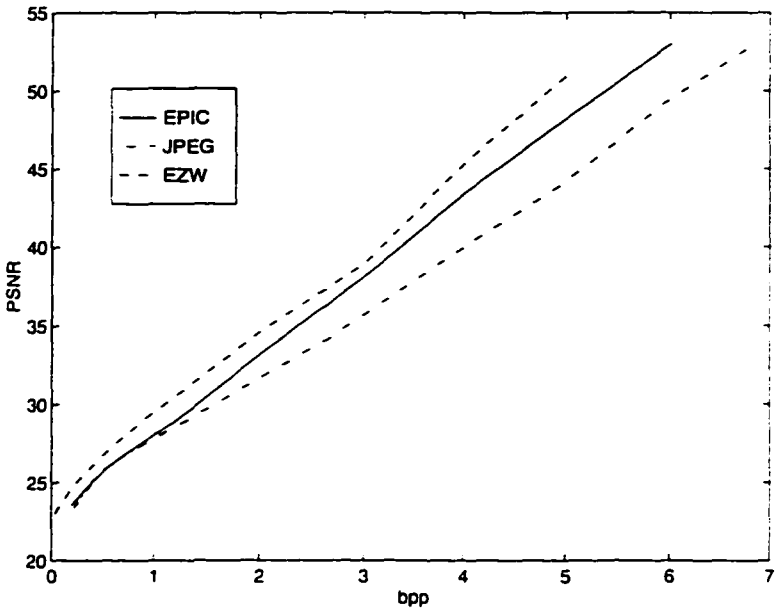

Figure 4.7: Comparison of three compression algorithms on the orginal *ext1* image.

Chapter 5

Speckle Noise Reduction Using Selective Wavelet Coefficient Soft-thresholding

5.1 Introduction

We have shown in the previous chapter that speckle noise tends to weaken or break the intra- and inter-band correlation in SAR images. As a result, it prohibits the effective compression of SAR images. Therefore, it is desirable that speckle noise be eliminated or at least reduced prior to image compression. While many researchers have worked on the smoothing of speckle noise using spatial domain techniques, we will follow a different approach in which speckle noise reduction is performed in the wavelet domain.

Wavelet domain noise reduction is a relatively new research concern. Pioneer work in this area includes Mallat and Hwang [33], and Xu *et al* [55], in which continuous wavelet transforms were used. Another approach, named

wavelet coefficient soft-thresholding, was proposed by Donoho [16]. As previously discussed, this method performs soft-thresholding on discrete wavelet transform coefficients and has obtained promising denoising results for one dimensional signals with additive noise. But, in our experience, when applied to two dimensional signals, this method has the tendency to oversmooth both noise and signals, as will be discussed later.

In this chapter, we present a refined soft-thresholding approach. This approach makes use of the correlation structure of the wavelet coefficients to select edge coefficients in the wavelet domain and then protects them from soft-thresholding. Consequently, noise smoothing and edge preserving goals can be achieved simultaneously.

5.2 Correlation Structure of Wavelet Coefficients

An orthogonal wavelet transform projects a signal onto a set of orthogonal basis functions. The energy of a signal is concentrated onto only a few wavelet coefficients. Coefficients with larger values usually indicate the positions of rapid changes (edges) in the signal, and small coefficients usually correspond to detail information. While this is always the case for clean images, wavelet coefficients for noisy images are inevitably contaminated by noise and can hardly be used to identify edges directly. Thus, alternative ways should be investigated.

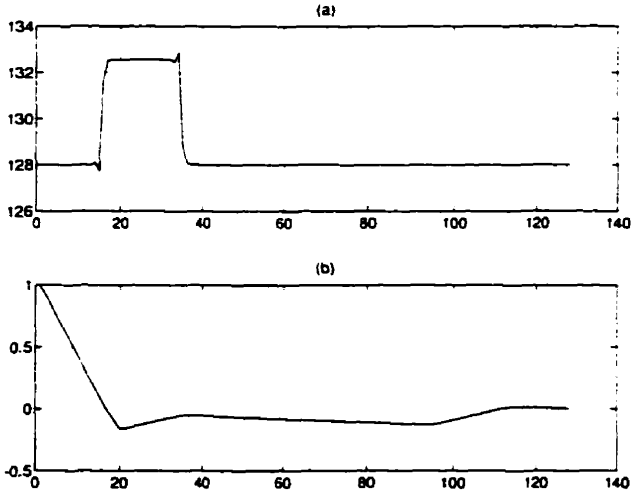

Figure 5.1: Correlation between adjacent pixels within the same resolution band: (a) A segment of wavelet coefficients from the decomposed *stripe* image; (b) The autocorrelation of (a).

Compared with many other transforms, such as the discrete cosine transform or discrete Fourier transform, an orthogonal wavelet transform does a better job in decorrelation. But the resulting wavelet coefficients are not totally uncorrelated. As proved by Dijkerman and Mazumdar, the correlation between orthogonal wavelet coefficients decreases exponentially rapidly across scales and hyperbolically along time (space) [15]. From an image processing point of view, we can make use of this short term correlation to select informative image features even in the presence of the uncorrelated noise which, after an orthogonal or bi-orthogonal transform, remains uncorrelated.

Fig. 5.1 shows (a) a segment of wavelet coefficients from the decomposed

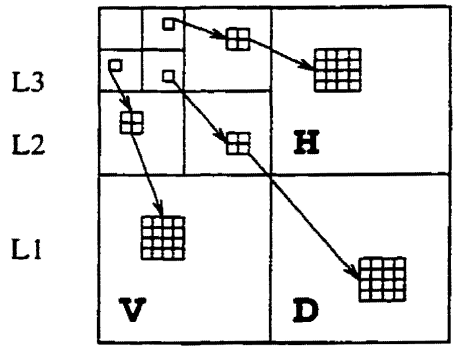

Figure 5.2: Definition of complete quadtrees.

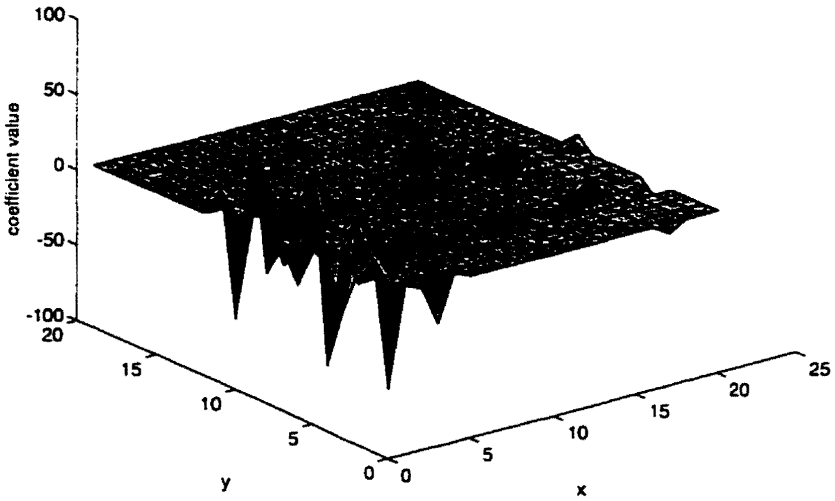

Figure 5.3: Illustration of inter-band correlation in quadtrees of *balloon* image with a total of 20 3-level quadtree given.

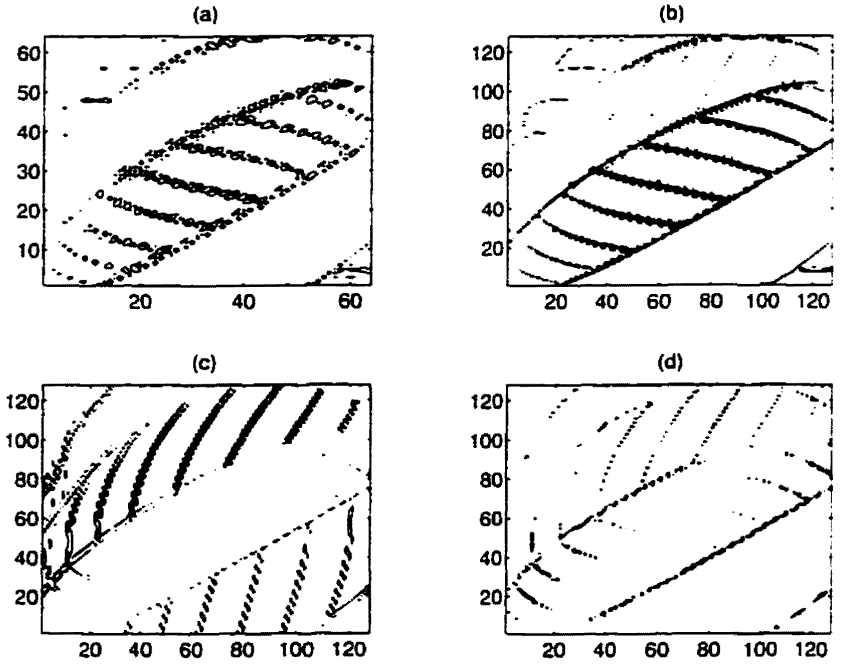

Figure 5.4: Contour maps of the coefficients from the decomposed *balloon* image shown in Fig. 3.3-(b): (a) contour map of subimage 2H (expanded to the same size as (b), (c) and (d)); (b) contour map of subimage 1H: (c) contour map of subimage 1V; and (d) contour map of subimage 1D.

stripe image at the same scale, and (b) the autocorrelation of (a). Coefficients corresponding to edge pixels possess large values in the wavelet domain. For an edge with a certain duration, it generates a large correlation value along the edge orientation. But this intra-band correlation becomes faint as the distance between the time (space) locations of the coefficients increases. For other isolated large coefficients induced by noise, due to the random nature of noise, they may not have significant correlation values. To illustrate the inter-band correlation, we group together the coefficients along quadtrees as

shown in Fig.5.2. For a particular decomposition level, say 3, each quadtree consists of 21 coefficients which correspond to the same spatial location. Fig 5.3 depicts 20 quadtrees taken from the *balloon* image in a 2-D graph. Each cross-section along the x-axis is one quadtree starting from the large scale root towards the finest scale leaves. As large coefficients in the wavelet domain correspond to edges in the spatial domain, we see that large coefficients appear over many scales, indicating that strong inter-band correlation exists among coefficients at different scales.

Fig. 5.4 shows the contour maps of the coefficients from the decomposed *balloon* image. They are generated by MATLAB in order to highlight the different edge extraction capabilities of each subimage. It should be noted that while large structures can be found in many scales, small image details can only be revealed in several fine scales (see Fig. 5.4-(a) and (b)). Thus calculating inter-band correlation involving only partial instead of entire quadtree elements is more reasonable. Fig. 5.5 shows the definition of partial quadtrees. Here, each quadtree is composed of coefficients from two adjacent scales. Besides, we see that when an orthogonal or bi-orthogonal wavelet transform is adopted, horizontal, vertical and diagonal subimages are generated which are quite different in their edge extraction abilities, i.e., oriented edges can only become visible in certain subimages (see Fig. 5.4-(b),(c) and (d)). This suggests that subimages of different orientations should be treated separately. Therefore, in the following context, the same procedure

is applied to the horizontal (H), vertical(V) and diagonal (D) subimages separately.

5.3 Definition of Hierarchical Correlation

From the above discussions, we can introduce the concept of hierarchical correlation which takes into account both the near neighbor intra-band correlation and the adjacent inter-band correlation along partial *quadtrees*(see Fig.5.5) which is a group of five wavelet coefficients corresponding to the same spatial location. For any two levels in the wavelet decomposition, the hierarchical correlation is defined as

$$correlation = \sqrt{r_1 \cdot intra} \tag{5.1}$$

$$intra = \begin{cases} max(\sqrt{t_1 \cdot t_2}, \sqrt{t_3 \cdot t_4}) & H - orient \\ max(\sqrt{t_1 \cdot t_3}, \sqrt{t_2 \cdot t_4}) & V - orient \\ max(\sqrt{t_1 \cdot t_4}, \sqrt{t_2 \cdot t_3}) & D - orient \end{cases} \tag{5.2}$$

where r_1 is one coefficient in the coarser scale and t_1, t_2, t_3 and t_4 are four coefficients in the next finer scale. Notice that the intra-band correlation is computed differently according to the orientation of the subimages involved. Oriented edges will generate larger correlation values and will be detected by this definition. A *correlation map* whose size is a quarter of the original image is then obtained because coefficients in the finest scale have no descendants. Large coefficients in this map indicate the position of edges in the original image, and zero coefficients correspond to smooth areas. The left-top part of the correlation map which corresponds to the lowpass subimage in the

wavelet decomposition will not be computed since we consider the coarsest resolution subimages are *clean* enough and as such, could be left unprocessed. Fig.5.6 shows an example of how correlation maps of the *stripe* image evolve along with the number of iterations.

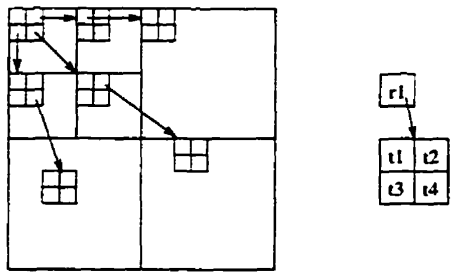

Figure 5.5: Definition of partial quadtrees.

5.4 Correlation Based Selective Noise Reduction Algorithm

Now we use the correlation map to distinguish edges from noise and then perform selective soft-thresholding on the wavelet coefficients. Our correlation definition allows fine structures which do not appear as local maxima to be revealed in the correlation map. This correlation map can then be used as an edge position indicator in the wavelet domain; thus pixels within quadtrees which are not selected as edges for certain thresholds are smoothed as noise. The algorithm is designed as an iterative one starting with a relatively small threshold which is increased on each iteration to gradually eliminate noise. The horizontal, vertical and diagonal orientations are processed separately

because oriented edges will only emerge in certain orientations. The complete processing procedure is given as follows:

Selective Soft-thresholding Algorithm

1. Perform logarithmic operation on the original image to convert multiplicative noise into additive noise.

2. Apply bi-orthogonal wavelet transform with maximum possible decomposition level.

3. (a) Compute correlation map.

   (b) Perform selective soft-thresholding on non-edge quadtrees.

$$\eta_t(v_i) = \begin{cases} v_i - t & v_i > t \\ 0 & -t \leq v_i \leq t \\ v_i + t & v_i < t \end{cases}$$

   (c) Stop if a stopping condition is reached. Else increase the threshold for edge detection and return to 3a and operate on $\eta_t(v_i)$.

4. Apply inverse wavelet transform.

5. Perform exponential operation.

Two thresholds are employed in the above algorithm. One is that used to determine edges from the correlation map. If the value of a coefficient is larger than the threshold, it is determined as edge, otherwise, it is treated as noise. A low threshold is initialized at the beginning to select many

coefficients as edge, and it is increased by a small value in each of the following iterations to eliminate noise gradually which is a conservative approach for the time being. Another threshold is used for the soft-thresholding. From our experience, the universal threshold obtained from Donoho's formula tends to oversmooth images. Currently there is no other well defined criterion for threshold selection. In this algorithm, we use the empirically obtained values of 0.5 or 1 for the threshold parameter for the lowest scale we are processing, and increase it by a small value (e.g., 0.5) to process smaller scale subimages.

There are two ways to stop this algorithm. One is to specify the number of iteration times. We find 10–15 iterations with threshold increment 0.5 per iteration can yield good noise reduction results for most of the test images used in our study. Alternatively, the algorithm can be stopped when a certain percentage of image pixels within an image are determined as edges. Thus this algorithm trades off preserving image details and reducing noise. These two conditions should be adjusted for different images according to image type and complexity.

We end by noting that Donoho's soft-thresholding idea has been implemented by Odegard *et al* [36] in speckle noise reduction. In their approach all the wavelet coefficients are soft-threshold processed. While speckle noise is reduced by this method, the subtle edges are also destroyed by this indiscriminate processing. The algorithm proposed in this thesis attempts to overcome this problem by performing selective wavelet coefficients soft-

thresholding, thus better preserving edge structures. The speckle smoothing results of these two approaches will be compared in the next setion.

5.5 Test Results on Simulated Speckled Images

In this part, we apply the proposed noise reduction algorithm on simulated speckled images. The purpose of this investigation is to gain insight into the selection of appropriate parameters for processing SAR images. Test results on real SAR images are to found in Chapter 7.

We start with the relatively simple image *stripe*. The noise-free version of this image (see Fig. 5.7(a)) consists of several vertical bars of different widths. It is then corrupted by multiplicative Gaussian noise of standard deviation 0.26 (shown in Fig. 4.2(b)). Fig. 5.6 shows the evolution of correlation maps along with increasing numbers of iterations. In these images, black pixels represent low correlation coefficients while white pixels indicate the positions of high correlation coefficients. We see that edge coefficients emerge gradually from the noise coefficients. Therefore, we can keep these prominent coefficients from soft-thresholding. As a result, image structures can be preserved while noise is smoothed.

Fig. 5.7 (b)–(d) shows the tests results on the simulated *stripe* image using Lee's multiplicative speckle filter, Donoho's overall soft-thresholding and the proposed selective soft-thresholding speckle filter. Because there are

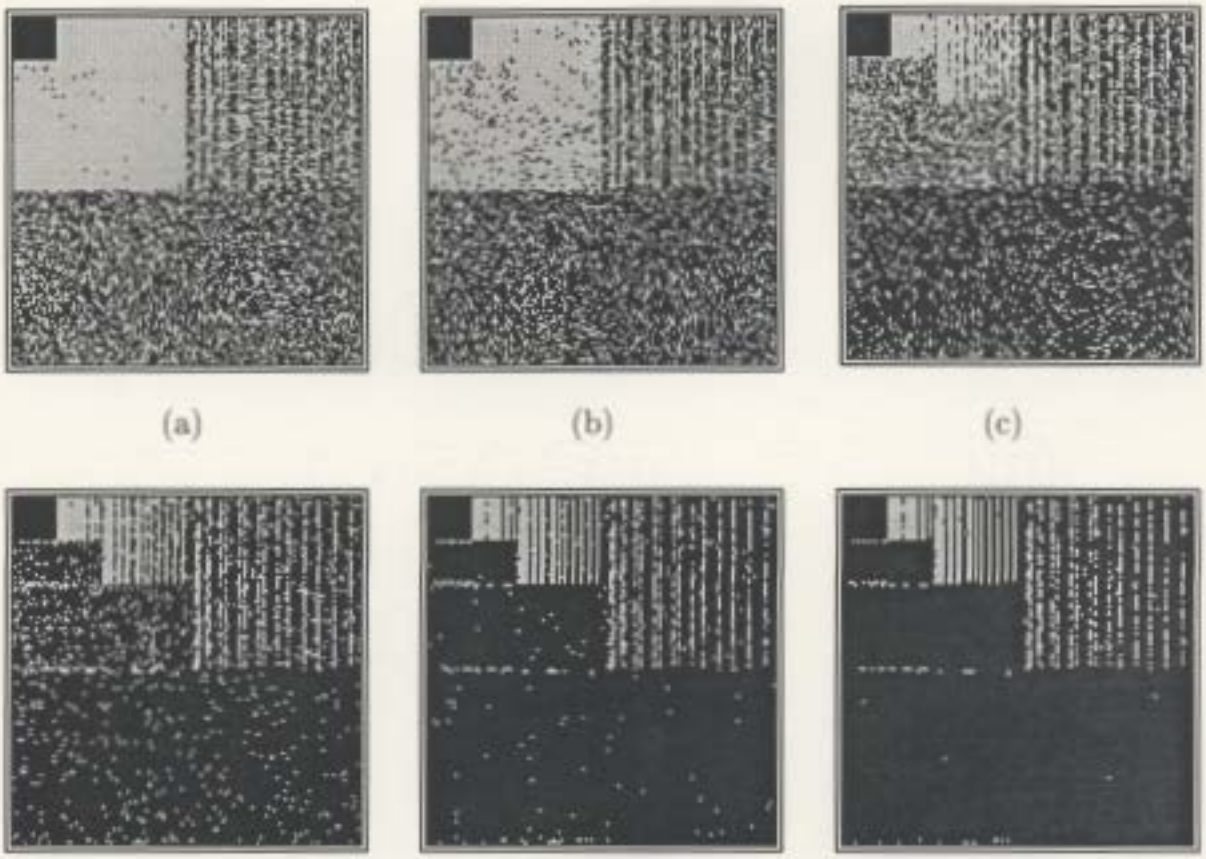

Figure 5.6: Correlation maps after (a) 1, (b) 4 , (c) 8, (d) 12, (e) 16 and (f) 20 iterations of the speckled *stripe* image. The size of these correlation maps is a quarter of the original *stripe* image.

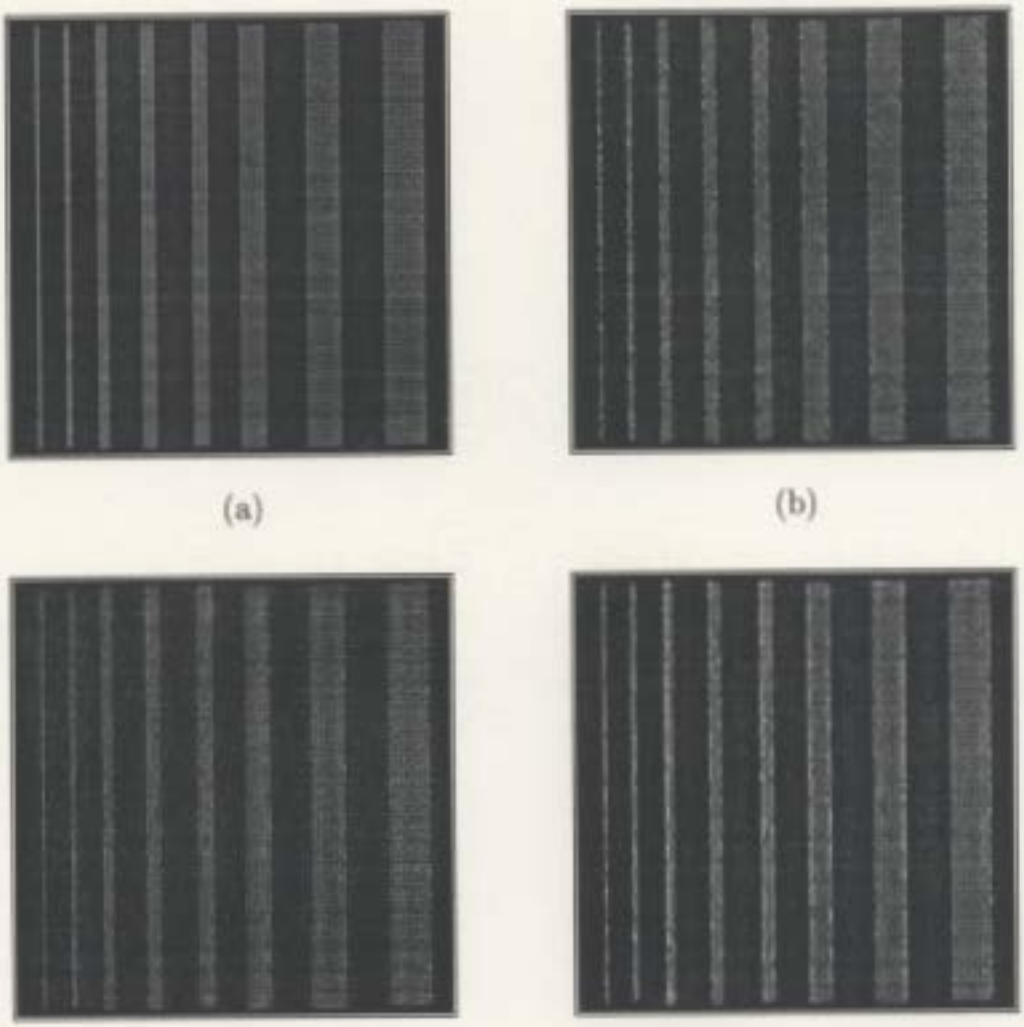

Figure 5.7: Comparison of speckle filtering results: (a) original; (b) Lee multiplicative filter; (c) Donoho's soft-thresholding; (d) selective soft-thresholding.

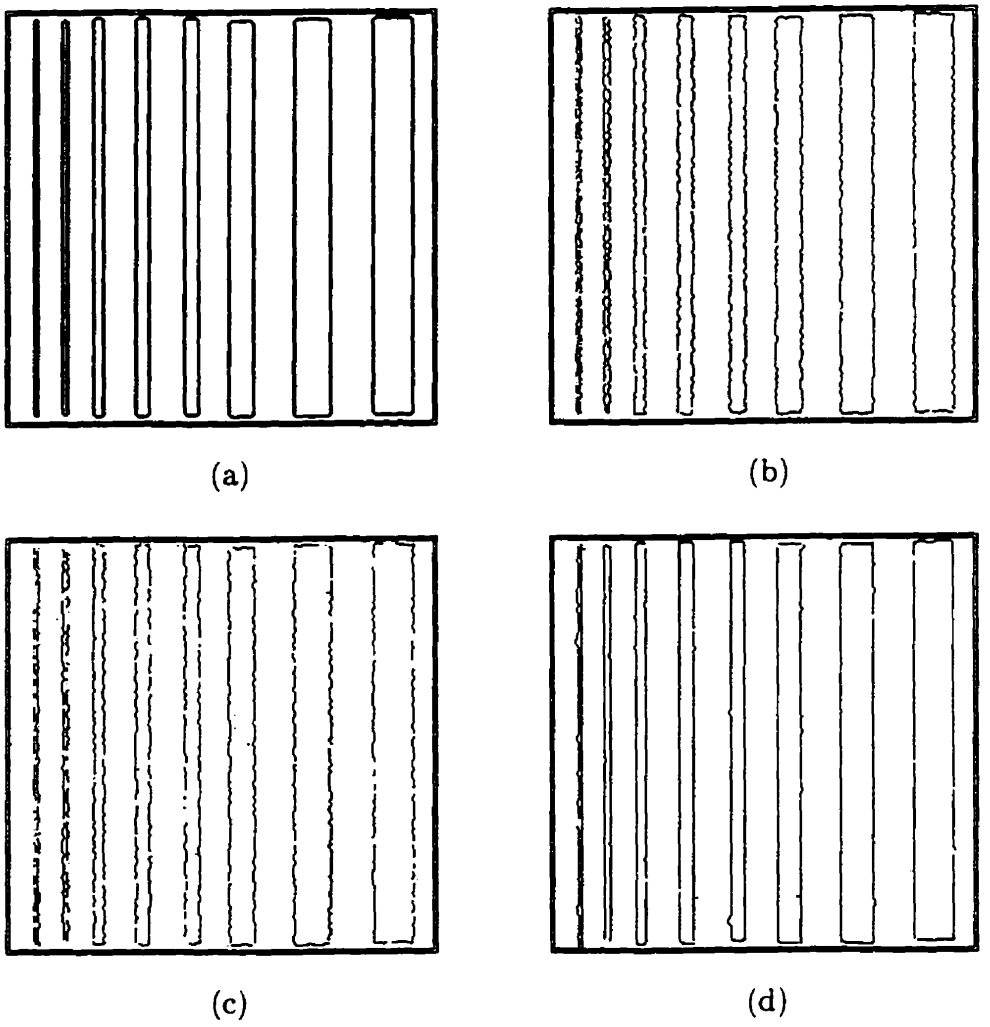

Figure 5.8: Comparison of edge maps for images of Fig. 5.7 (generated by MSPRoA, mask size=3, threshold=.55, correlation=1).

large homogeneous regions in this image, we use a large 7×7 mask for the Lee multiplicative filter. The mask size could be larger in order to better smooth the homogeneous regions, but then edges would start to go. The threshold used in Donoho's overall soft-thresholding is 3 which is also a trade-off between noise smoothing and detail preserving. The selective algorithm is iterated 20 times with starting correlation threshold 2 and increment 1. The threshold for soft-thresholding is set to 1 for this algorithm based on our experience.

We can see that visually, both the overall soft-thresholding and selective soft thresholding techniques can reduce speckle noise (the MSE value is reduced from 605 to 334 and 244, respectively). However, Donoho's overall soft-thresholding smoothes both edge and noisy pixels, and the resulting image looks blurred. The filtering result obtained from the proposed selective soft-thresholding has a much brighter appearance with enhanced edge sharpness, and the thin edges are well preserved. The smoothed image produced by the well-known Lee multiplicative speckle filter is provided for comparison. While this filter works fairly well in homogeneous areas, it is not capable of removing the noise in the edge regions effectively; there is still substantial noise left on those thin bars. Fig.5.8 further shows the corresponding edge map of these images generated by the MSPRoA edge detector [20] which is an edge detector specially designed for speckled images. More details on the use of the MSPRoA edge detector, including the setting of parameters and

their robustness can be found in [20]. In Fig. 5.8. Fig. 5.9. etc. we have used appropriate sets of parameters. It is not surprising that the selective soft-thresholding method can produce the best edge map because it has the built-in feature to protect and enhance oriented edges.

Fig. 5.9(a) shows another image *airfield*. We have reduced the contrast of this image in order to prevent saturation when corrupting it by multiplicative noise (MSE=303.79). Fig. 5.9(b) and (c) are the processing results from the Lee multiplicative filter (MSE=44.33) and the selective soft-thresholding (MSE=77.23), respectively. Visually, we may consider that the Lee multiplicative filter produces better result than the soft-thresholding approach. This may be due to the nature of soft-thresholding which shrinks the dynamic range of image intensity and therefore reduces image contrast. Thus quantitatively, the soft-thresholding methods produce filtering results with higher mean-square-error than the Lee multiplicative filter or other filters. But again, speckle noise near edge regions is not smoothed by the Lee multiplicative filter. We should also note that the proposed selective filter cannot handle strong impulse noise which may appear in homogeneous regions as effectively as the Lee multiplicative filter where a large mask size can be adopted for this situation. Thus from the filtered image, we can observe some burst-like noise. In this case, we can use a median filter with a small 3×3 mask to further eliminate residual noise and obtain an filtered image with better visual quality and slightly blurred edges (Fig. 5.9(d)).

Finally, it is worth noting that because the proposed correlation based algorithm enhances both the inter and intra band correlation, better compression performance could be expected for speckle reduced images. We leave the discussion related to this issue to Chapter 7.

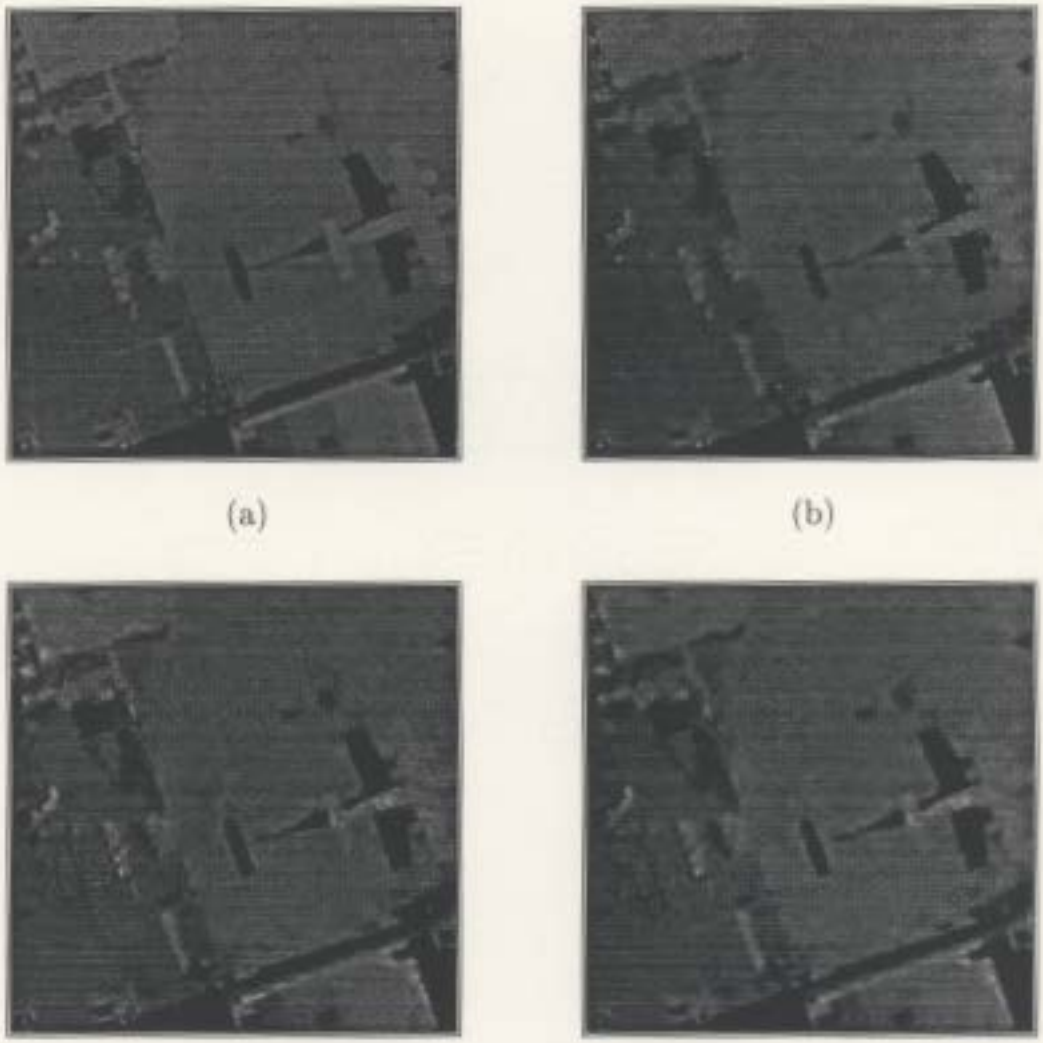

(a) (b)

(c) (d)

Figure 5.9: Comparison of filtering results. (a) Original noise-free image *airfield*, (b) Lee Multiplicative filter; (c) Selective soft-thresholding; (d) (c) after 3×3 median filter.

Chapter 6

Multi-rate SAR Image Compression Using Zerotree Wavelet Coding

6.1 Introduction

Apart for speckle noise, another key characteristic of SAR images is the large variation in image contents. Because the resolution cell for SAR images are much larger than that for optical images, a SAR image can cover a large area of terrain and there can be a variety of scene contents within an image which convey information of different importance to different viewers. When a SAR image is requested, people may only want to get some large scale information, such as the course of a river or positions of some important objects. On the other hand, people may wish to focus on several small regions. Because the transmission of a large size SAR image in full resolution can be remarkably slow, compressing different regions with multiple bit rates and thus creating

an image with multiresolution is desirable.

In this chapter, we implement a multi-rate compression scheme based on the EZW algorithm. Although there are many issues related to this topic which require further investigation, we believe that the multi-rate compression scheme will facilitate efficient transmission of large size SAR images.

6.2 The Multi-rate EZW Compression Scheme

Progressive transmission is often desired for browsing purposes. A lowpass image is received at the beginning of transmission for quick reference and more details are added upon the viewer's request. Embedded coding algorithms are natural suited for this purpose. In an embedding coding algorithm, at the beginning of the bit stream the embedded code contains the lower bit rate code. That is, decompressing this initial bit stream will generate a low resolution approximation image with a relatively few data. As the decoding continues, more and more fine details will be received in the order of importance to produce a reconstructed image with increasingly higher and higher resolution.

A multi-rate compression scheme is built on top of an embedded coding algorithm. It makes use of the embedding property of the embedded compression algorithm in order to further enhance transmission efficiency. If the compression is based on a wavelet transform, then given the locations of regions of interests, we can determine the locations of those wavelet coefficients

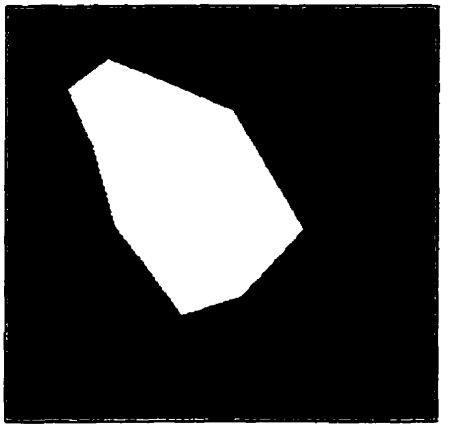

Figure 6.1: Region mask in the spatial domain.

associated with these regions. Thus we can simply ignore the parts of the bit stream not related to the regions of interest and obtain a reconstructed image of these regions more rapidly.

Assuming the locations of the regions of interests are pre-specified, the straightforward way to split and encode different region is to partition pixels of the raw image in the spatial domain. For the simplest case, an image is partitioned into two regions, labeled as the interior and exterior regions (see Fig. 6.1). In order to be processed by conventional algorithms, these two regions are overlaid onto two blank images of the same size as the raw image (see Fig 6.2). These two resulting images are then encoded separately, producing two data streams. At the reconstruction side, these two streams are decoded separately. The final image is obtained by summing the two decoded images (Fig. 6.3).

This spatial domain partition scheme has two disadvantages. First, since

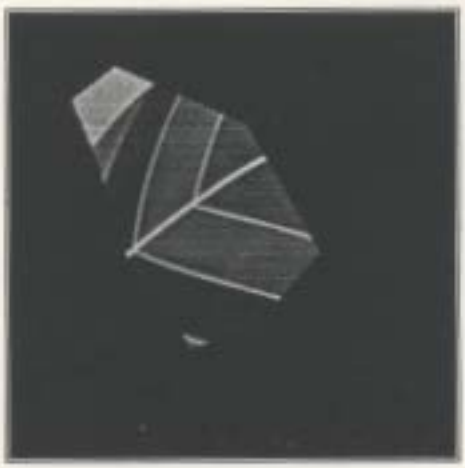

(a)

(b)

Figure 6.2: Spatial domain partition for the *balloon* image of Fig. 3.3-(a): (a) interim region 1; (b) external region 2.

Figure 6.3: Reconstructed image from the spatial domain partition.

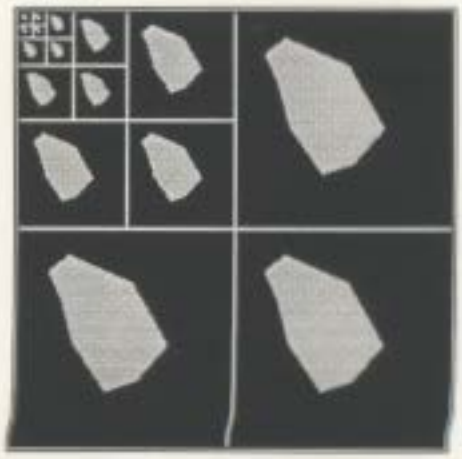

Figure 6.4: Region mask of Fig. 6.1 in the wavelet domain (5 level decomposition).

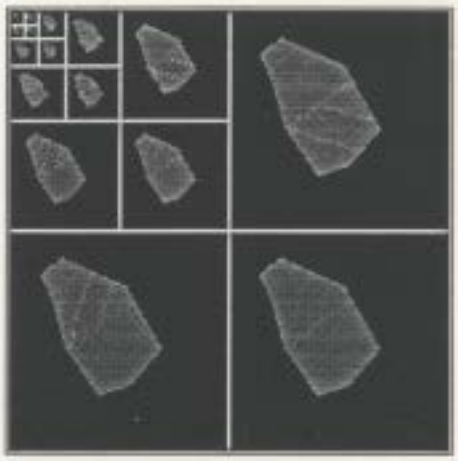

(a)

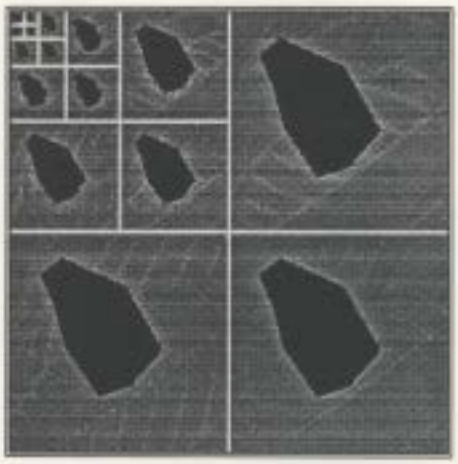

(b)

Figure 6.5: Wavelet domain partition: (a) interim region 1; (b) external region 2.

Figure 6.6: Reconstructed images from the wavelet domain partition.

the two partitioned images are processed totally independently, each of them needs a pass of both the wavelet transform and inverse wavelet transform, and these respective blank regions are unnecessarily processed too. Second, there are artifacts near the region boundary in the reconstructed image due to the boundary effect of the wavelet transform (see Fig. 6.3).

An alternative is to partition these regions in the wavelet domain (see Fig. 6.4). Because a direct correspondence exists between the raw image and its subbands, it is easy to pick up the region of interest in the wavelet domain (see Fig. 6.5). Thus only one pass of the forward and inverse wavelet transform is required regardless how many regions are specified. Each region can then be encoded separately and each data stream only contains the information about the specific region. At the decoder, each data stream is decoded individually, and they are fused in the wavelet domain. This can avoid the boundary effect (see Fig. 6.6) and the process will be faster.

It should be noted that for the multiple rate compression scheme. the region mask should be available at both the encoder and the decoder. The transmission of mask may add to the transmission load. but is relatively insignificant compared with the overall data reduction. It should also be pointed out that the spatial domain partition is more robust than the wavelet domain partition scheme because the latter may be more vulnerable to transmission errors.

6.3 Implementation of Multi-rate Compression Scheme Based on EZW

6.3.1 Implementation of The Original EZW Algorithm

The EZW is a state-of-the-art image compression algorithm. We consider this algorithm to be a good candidate for SAR image compression because the embedded nature of this algorithm naturally facilitates progressive transmission. In addition, as we have seen in Chapter 4, the EZW and other algorithms which make use of the inter-band correlation of wavelet coefficients suffer less from speckle noise than other run-length coding based compression algorithms. Thus we designed our multi-rate compression scheme based on the EZW algorithm.

We have described the EZW algorithm in Chapter 3; more details can also be found in [42, 44]. We summarize the algorithm into the following procedure. First we note some of the notation used in the algorithm descrip-

tion.

Notations:

- $c_{i,j}$ - the wavelet coefficient at position (i, j).
- $S_n(i, j)$ - significance indicator at position (i, j); if coefficient $c_{i,j}$ has significant descendant(s) or itself is significant, $S_n(i, j) = 1$. otherwise. $S_n(i, j) = 0$.
- LSP - list of detected significant coefficients.
- LIP - list of insignificant coefficients.
- LIS - list of insignificant zerotrees.
- n - numbers of successive approximation operations needed.

Said and Pearlman's EZW Algorithm

1. **Initialization**: Compute $n = \lfloor \log_2(max_{(i,j)}\{|c_{i,j}|\}) \rfloor$; set the LSP as an empty list; add all the roots of the quadtrees to LIP and LIS.
2. **Sorting pass:**
   (a) for each entry in LIP:
   - encode $S_n(i, j)$;

- if $S_n(i,j) = 1$, move coefficient (i,j) to LSP.

(b) for each entry in LIS,

- encode $S_n(i,j)$;
- if $S_n(i,j) = 1$, move the descendant(s) to LSP.[1]

3. **Refinement pass:** for each entry (i,j) in LSP, except those detected in the last sorting pass (i.e. with the same n), encode the most significant bit of $|c_{i,j}|$;

4. **Quantization-step update**: decrement n by 1 and goto step 2.

To describe the decoding algorithm, we only need to replace the "encode" with "decode" in the above algorithm. Note that when the decoder decodes data, its three lists (LSP, LIP, and LIS) are identical to the ones used by the encoder at the moment it encoded that data. This means that the decoder indeed recovers the ordering information from the execution path. With this highly symmetric scheme, the encoding and the decoding have the same computational complexity.

6.3.2 Implementation of Multi-rate Scheme

Currently, we assume that the regions are pre-defined, and the region mask is available at both the sender and the receiver. Making use of the relation between wavelet coefficients and their corresponding spatial positions, we can

[1] In fact, Said and Pearlman's algorithm further differentiates LIP into two types from the implementation point of view. We skip the discussion here.

generate masks in every subimage as shown in Fig. 6.4. After the wavelet domain partitioning, we encode each region using EZW into a separate data stream. At the receiver, we decode each of the data streams and recover the corresponding regions in the wavelet domain. Finally, we recover the image by the inverse wavelet transform.

The complete multi-rate compression scheme can be implemented by the following procedure. First, we define some more notations.

Notations:

- N - number of regions
- R_k - region k
- b_k - bit rate for R_k
- S_k - bit stream corresponding to R_k

Multi-rate EZW Encoding Algorithm

1. **Initialization:**
   - read in the *spatial_mask* (which should be the same size as the the original image);
   - specify bit rate for each region, $b_1, b_2, \cdots$ and b_N;

2. **Mask generation in the wavelet domain:**

   - compute the decomposition level;
   - highlight the masked region in the wavelet domain and obtain the *wavelet_mask* for the partitioned regions $R_1, R_2, \cdots$ and R_N.

3. **Wavelet transform** The original image is converted to wavelet domain.

4. **Encoding:** for each wavelet coefficient $c_{i,j}$,

   - if $c_{i,j} \in R_k$, encode this coefficient with bit rate b_k using EZW. Append the encoded coefficient to bit stream S_k.
   - if the bit budget for region R_k has been exhausted, skip this coefficient.

5. **Transmission of several data streams** The encoded data streams can be transmitted sequentially or in parallel.

Multi-rate EZW Decoding Algorithm

1. **Initialization:**

   - read in the *spatial_mask* (should be the same size as the original image);

- specify bit rate for each region, $b_1, b_2, \cdots$ and b_N;
- decode stream header.

2. **Mask generation in the wavelet domain:**
   - restore the decomposition level;
   - highlight the masked region in the wavelet domain and obtain the *wavelet_mask* with partitioned region $R_1, R_2, \cdots$ and R_N.
3. **Decoding:** for each of the received wavelet coefficients $c_{i,j}$ from data stream S_k,
   - decode this coefficient with bit rate b_k using EZW. Assign the decoded coefficient to region S_k.
   - if the bit budget for stream S_k has been exhausted, skip this coefficient.
4. **Inverse wavelet transform.** The image is recovered with specified bit-rates (resolution) for the different regions.

It should be noted that because the EZW organizes the wavelet coefficients into a tree structure, if the large scale coefficients are skipped, all their off-springs in smaller scales will not be processed. As a result, the processing time is reduced.

6.4 Discussion

The parameters of the multi-rate compression scheme include shape, size and number of the regions, and the specification of the bit rate for each region. In the above discussion, we use region masks to specify regions. An irregular region mask is used to demonstrate the multi-rate scheme. This is to simulate the regions generated by image segmentation where an image is segmented into several irregular regions according to pixel intensity or texture. Although we use a two-region case as an example, the extension to more regions is straightforward. Because currently we use the same pixel intensity to represent a region, more regions can simply be represented by more intensity levels, but the algorithm itself is unchanged.

We are more likely to select rectangle regions when browsing an image. This results in a simplified version of the multi-rate compression scheme. In this situation, the transmission cost of mask information, such as mask size and shape can be greatly reduced.

The bit budget for each region can be as low as 0, but no greater than bpp_{max}, where bpp_{max} can be calculated as

$$\text{bpp}_{\text{max}} = \frac{\text{number of total pixels}}{\text{number of pixels in this region}} \times \text{given bpp} \qquad (6.1)$$

The multi-rate compression scheme is intended to provide efficient transmission of SAR images. This scheme can be combined with the selective soft-thresholding proposed in the last chapter to achieve noise reduction and

image compression tasks simultaneously. Technically, noise reduction can be performed before the multi-rate EZW compression or inserted in the compression algorithm just before the encoding operation. However, due to the difficulties in setting appropriate processing parameters for the selective soft-thresholding method, presently we separate these two operations in two steps, i.e. first we use the selective soft-thresholding method to do the speckle suppression, then we compress the de-noised image with the multi-rate EZW algorithm. We expect that after having gained enough experience with noise smoothing of SAR image, we can finally combine these two steps in one complete noise smoothing and image compression algorithm.

Chapter 7

Test Results and Discussion

7.1 Introduction

Speckle noise and large dynamic range are two key characteristics of SAR images. In previous chapters, we developed the selective soft-thresholding technique and the multi-rate compression scheme to compress SAR images effectively. We have tested these methods on simulated speckled images generated using the simple multiplicative speckle model. In this chapter, we test these methods on real SAR images, which can be modeled using a slightly more complete speckle model and have more complicated scene contents. Tests are designed for three purposes: performance of the selective soft-thresholding method for speckle noise reduction; effects of speckle noise reduction on SAR image compression; and the effectiveness of the multi-rate compression scheme. In addition to the two SAR image extractions frequently used in previous chapters (see Fig. 4.1), we also introduce two larger SAR images with more complex image contents in our evaluations.

7.2 Tests on Speckle Smoothing of SAR Images

As we have shown in Chapter 4, speckle noise has inverse effects on SAR image compression. In order to compress SAR images more effectively, in Chapter 5 we proposed the selective soft-thresholding method to smooth speckle noise and enhance inter-pixel correlation in SAR images. In this section, we will demonstrate the speckle smoothing effects of the proposed method on real SAR images.

Fig. 7.1 shows the filtering results of SAR extraction *ext1* and *industry* using the selective soft-thresholding method. The corresponding original images can be found in Chapter 4 (see Fig. 4.1). Clearly *industry* contains more details that *ext1*. Thus, *SST-ext1* (see Fig. 7.1-(a)) is obtained after 15 iterations while *SST-industry* (Fig.7.1-(b)) is obtained after 12 iterations. (c) and (d) are the MSPRoA edge maps of (a) and (b), respectively. In (a) and (b), the threshold for detecting significant coefficient starts from 1, and is increased by 0.5 per iteration. The threshold used for soft-thresholding is 1. The results obtained from the Lee multiplicative speckle filter (discussed in Section 2.4) are also shown for comparison (see Fig. 7.2). To trade off the noise smoothing and edge preservation, a moderate 5×5 mask size is used in the Lee filter, and since the test images are approximately 4-look, the noise standard deviation is chosen to be σ_v=0.26 [25]. All the edge maps generated by the MSPRoA detector [20] use mask size=5, threshold=0.6 and

correlation=1.

We see that visually both the Lee filter and the selective soft-thresholding method can reduce speckle noise, but they differ in their noise smoothing capabilities. In order to prevent oversmoothing fine details, we use a moderate size processing mask (5×5) in the Lee filter. From Fig. 7.2-(b), we find that there is residual noise left in the homogeneous regions due to undersmoothing. We also observe considerable speckle noise in edge regions which is not smoothed by the Lee filter. From Fig. 7.1-(b), we see that after a certain times of iterations, the speckle noise in homogeneous regions is significantly removed. We also see that the fine details near the building are fairly well preserved even after so many iterations, while these are blurred in the image obtained from Lee filter. We are convinced that since the selective soft-thresholding method has the feature of enhancing line features, it can be used to detect and enhance man-made structures. The edge maps of the smoothed SAR images further illustrate the edge preserving ability of the proposed method; the fine details are preserved and the homogeneous regions are smoothed.

Because there are no noise-free versions of the SAR images, we cannot use MSE or other similar objective measures to evaluate the noise smoothing performance. Instead, we manually choose several small regions (11×11) from the images which appear to be homogeneous to evaluate the noise smoothing effect in these regions. The mean, standard deviation and σ_v measures for

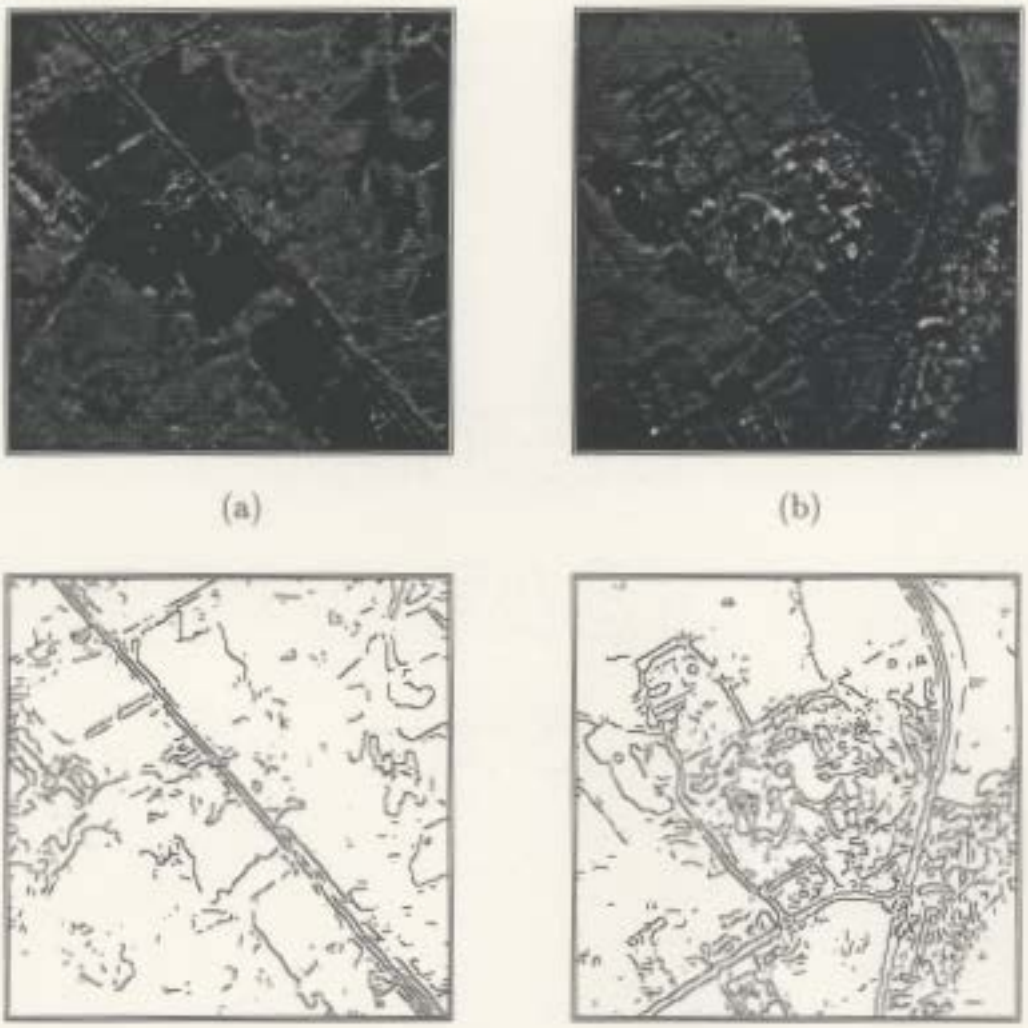

Figure 7.1: Speckle smoothing using selective soft-thresholding method. (a) *SST-ext1* (after 15 iterations); (b) *SST-industry* (after 12 iterations); (c) MSPRoA edge map of (a). (d) MSPRoA edge map of (b). ((c) and (d) are generated using mask=5, threshold=.6, D=1).

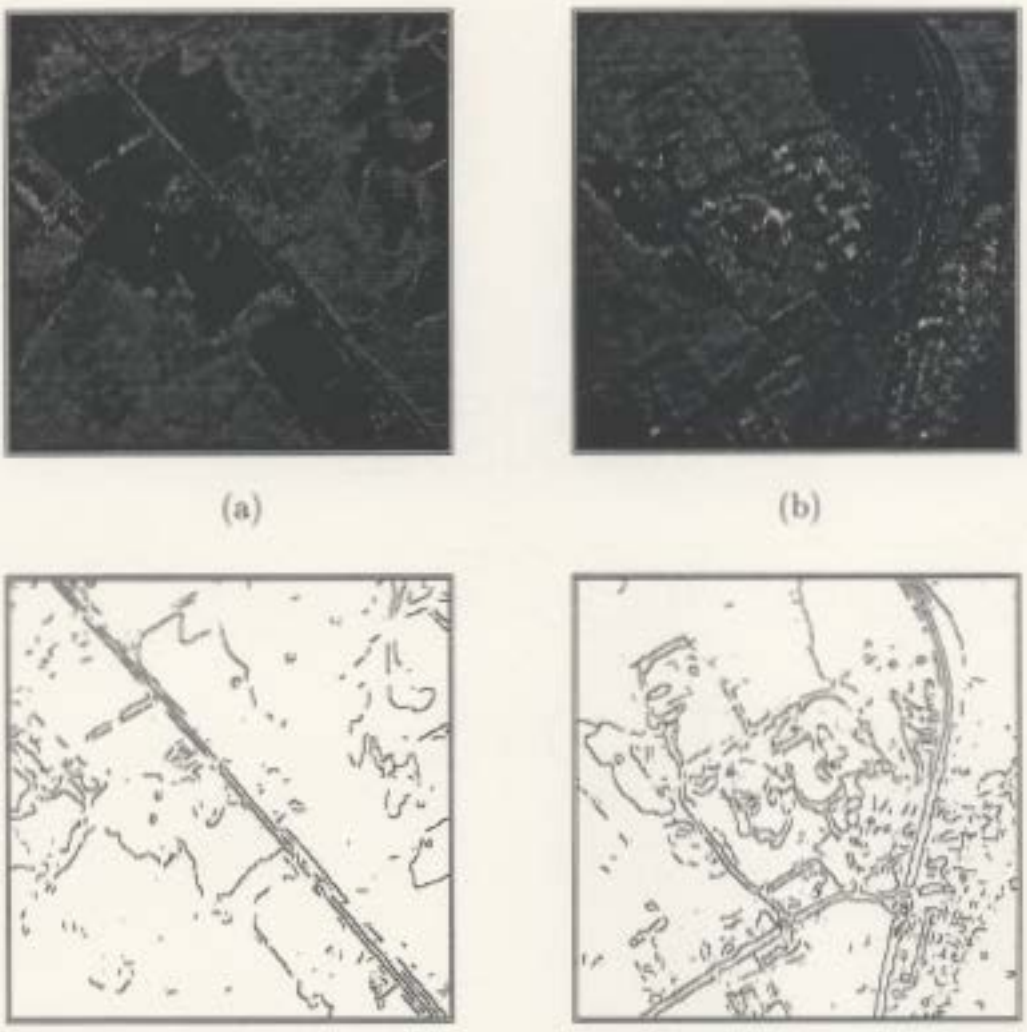

Figure 7.2: Speckle smoothing using Lee multiplicative filter. (a) and (b) are processed using mask size=5, σ_v=0.26. (c) MSPRoA edge map of (a); (d) MSPRoA edge map of (b). ((c) and (d) are generated using mask=5, threshold=0.6, D=1).

image	area1 (dark)			area2 (bright)		
	mean	var	σ_v	mean	var	σ_v
original	26.23	5.81	0.221	62.09	15.82	0.255
Lee (mask=5)	25.71	1.84	0.071	62.45	3.77	0.060
selective	23.85	1.77	0.074	57.52	3.66	0.064

image	area3 (edge)			area4 (edge)		
	mean	var	σ_v	mean	var	σ_v
original	35.80	21.61	0.604	48.88	28.63	0.586
Lee (mask=5)	35.00	17.57	0.502	46.60	23.59	0.506
selective	34.97	22.00	0.629	46.60	23.96	0.514

Table 7.1: Quantitative measures for noise smoothing of *ext1* image.

image	area1 (dark)			area2 (bright)		
	mean	var	σ_v	mean	var	σ_v
original	14.45	4.28	0.296	58.72	14.48	0.247
Lee (mask=5)	13.88	1.61	0.116	57.76	4.12	0.071
selective	12.93	1.09	0.084	53.87	3.05	0.057

image	area3 (edge)			area4 (edge)		
	mean	var	σ_v	mean	var	σ_v
original	50.95	20.01	0.393	22.06	13.29	0.602
Lee (mask=5)	50.39	14.32	0.284	21.37	10.90	0.510
selective	48.54	16.25	0.335	20.89	11.64	0.557

Table 7.2: Quantitative measures for noise smoothing of *industry* image.

two of these regions are shown in Table 7.1 and Table 7.2. In addition to these homogeneous regions, we also select two other regions which contain edge activity: the measures for these regions are also shown in Table 7.1 and Table 7.2. Thus for each smoothed image, we expect small variance and σ_v values for the flat regions both dark and bright, and large variance and σ_v values for edge regions. Again, we include those measures for the images obtained from the Lee filter for comparison. We see that for these two SAR image extractions, the proposed filter performs better overall than the Lee filter in both noise smoothing and edge preservation. From the edge maps of the filtered images we see that the treatment by the proposed filter of the edge pixels in these images preserves and enhances the edge structures. Thus the edge detector can generate more accurate edge maps for the smoothed images.

Fig.7.3 shows one real SAR image which contains various image contents. The size of this image is 750 × 680, which is much bigger than *ext1* and *industry* whose sizes are 256×256. The top-left and the bottom-right regions are terrains and coast lines while the vast center region is a ice-covered river. We may notice there are some quite faint ice cracks in the ice region. Fig. 7.4 shows the output of the proposed filter after 12 iterations. Speckle noise in the terrain regions is effectively removed and the fine details such as the roads are preserved. For the ice region, we can see that although it may be over-smoothed after so many iterations, some major ice cracks are still

visible. Compared with the result of Lee filter (Fig. 7.5). the result obtained from the selective soft-thresholding filter is quite encouraging.

Before we end the discussion of this section. we should note that although the proposed filter produces good results on the test images. it has some limitations. First, it is capable of detecting and enhancing line features in the images, but it does not perform equally well on features with short duration such as the point targets in the *ext1* image (see Fig. 7.1(a)). Second. currently the proposed method stops after having finished a certain number of iterations. For images with much edge activity, we perform fewer iterations to preserve image details while for relatively simple images, we can do more iterations. But for images with spatially varying complexity such as that of Fig. 7.3, we have to trade off the noise smoothing and detail preservation by using a moderate number of iterations. The issue of adapting iteration times to image statistics deserves further study.

7.3 Effect of Speckle Noise Reduction on Image Compression

In this part, we evaluate the effects of speckle smoothing using the selective soft-thresholding method on SAR image compression. JPEG, EPIC and the original EZW algorithms are used in the evaluation. We also use the EPIC and EZW measures defined in Chapter 4 in our evaluations. Some results obtained in Chapter 4 are referenced here for comparison.

Figure 7.3: Original SAR image *coast and river* with varied image content.

Figure 7.4: Smoothed *coast and river* image using the selective soft-thresholding method after 12 iterations.

Figure 7.5: Smoothed *coast and river* image using the Lee multiplicative filter with mask size=5×5.

Fig. 7.6, 7.7 and 7.8 show the reconstructed image quality as a function of bit-per-pixel rate for SAR images before and after speckle smoothing. We see that compared with the original speckled SAR images, the performance of all three compression algorithms on the speckle smoothed SAR images is significantly improved, indicating the effectiveness of speckle noise reduction on SAR image compression. We may notice that for high and moderate bit rates, the de-speckled SAR images can be better reconstructed at a given rate than can the speckled images. But when the bit rate becomes very low, the original and de-speckled image have comparable compressibility. This is because for such low bit rates, only the major structures in the images are encoded and both the noise and the fine details are eliminated, i.e., these compression algorithms also serve as a noise filter. Now we see that not only is speckle reduction profitable for image compression but compression itself is also a process of noise reduction.

Table 7.3 and Fig. 7.9 show the cross comparison of the three algorithms with their respective parameters. Among these three algorithms, we find EZW still has the best performance. At the same time, it may be interesting to find that for the de-speckled *ext1* and *industry* images, EPIC outperforms JPEG. As we discussed in Chapter 4, speckle noise weakens the inter-pixel correlation in SAR images and thus makes run-length coding based compression algorithms perform less effectively. Because the proposed speckle noise smoothing method suppresses the noise and enhances the inter-pixel correla-

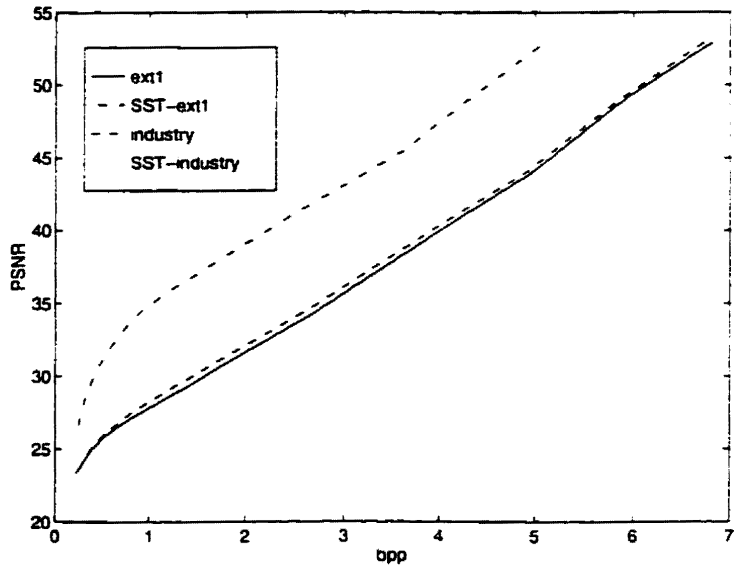

Figure 7.6: Comparison of compression performance on original and despeckled SAR images using the JPEG algorithm

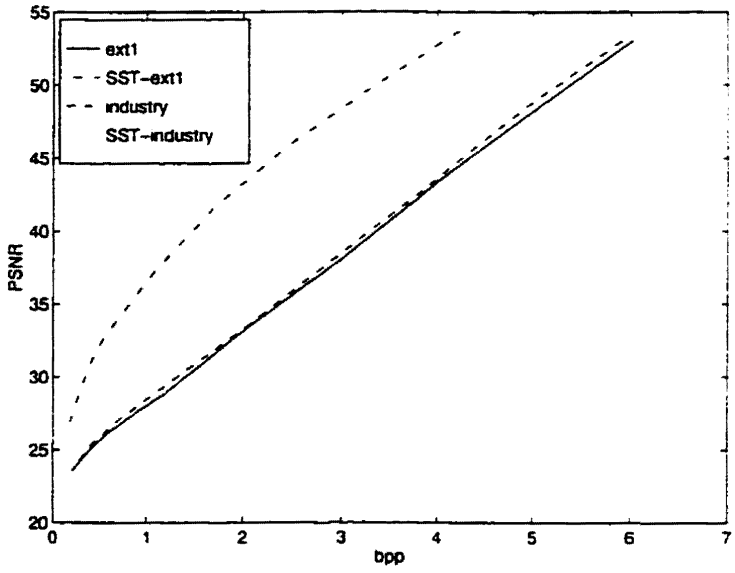

Figure 7.7: Comparison of compression performance on original and despeckled SAR images using the EPIC algorithm

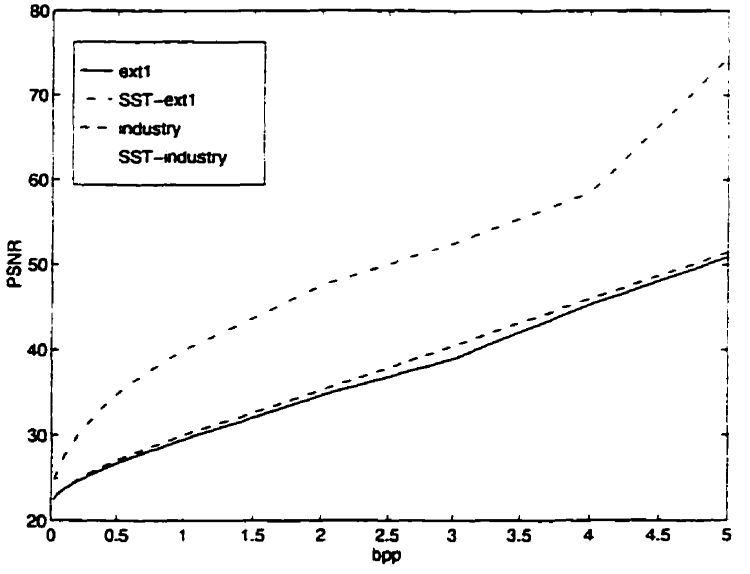

Figure 7.8: Comparison of compression performance on original and de-speckled SAR images using the EZW algorithm

tion among the wavelet coefficients, the simple wavelet based EPIC algorithm takes advantage of the enhanced correlation and thus is competitive with the JPEG standard. We can expect that the de-speckled SAR images can also be better compressed by other compression algorithms, especially those wavelet based algorithms.

Table 7.4 shows the run-length distribution for *ext1* and *industry* before and after speckle smoothing. The number of runs of length shorter than 10 is significantly reduced. Table 7.5 gives the EZW measures on de-speckled *ext1* and *industry* images. Because the selective soft-thresholding exploits both the inter and intra band correlation among the wavelet coefficients, the self-similarity of the image elements is enhanced. Thus we can find that

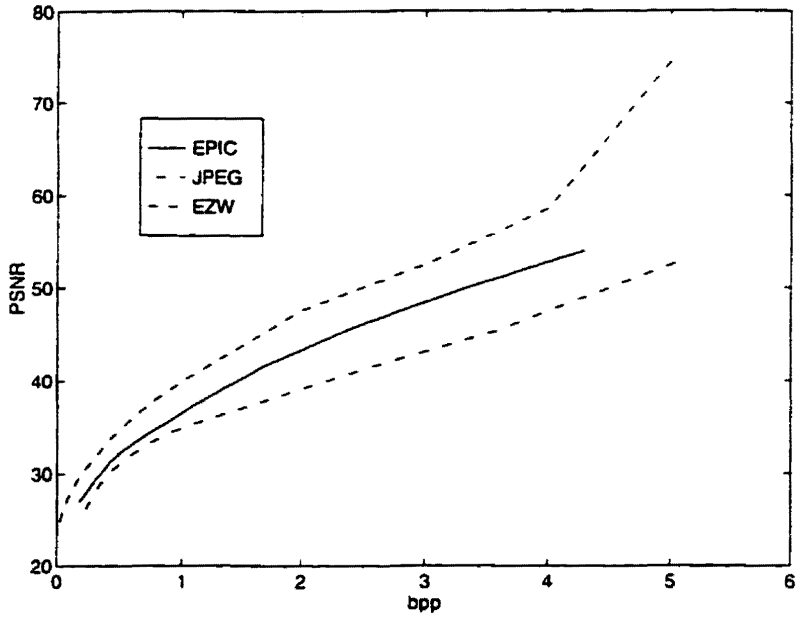

Figure 7.9: Comparison of three compression algorithms on the de-speckled *ext1* image.

	ext1					
	JPEG		EPIC		EZW	
measure	original	smoothed	original	smoothed	original	smoothed
bpp	1.65	1.12	1.77	0.95	1.5	1.5
PSNR	30.32	35.48	31.65	36.25	32.09	44.07
peak	45	35	28	26	31	9

	industry					
	JPEG		EPIC		EZW	
measure	original	smoothed	original	smoothed	original	smoothed
bpp	1.62	1.18	1.72	1.04	1.5	1.5
PSNR	30.70	34.81	31.86	35.61	32.58	42.48
peak	47	46	28	26	35	11

Table 7.3: Comparisons of compression performance on de-speckled SAR images.

Table 7.4: Comparison of the EPIC measure with test images. (bin=20. level=4)

measure	ext1		industry	
	original	smoothed	original	smoothed
0–10	8652	2733	8007	3011
11–20	666	441	735	407
21–30	232	188	229	177
31–40	127	125	111	123
41–50	36	63	61	84
51–60	18	53	27	51
61–70	4	39	12	40
71–80	3	18	3	32
81–90	0	25	1	30
91–100	0	21	0	22
>100	0	138	2	148

Table 7.5: Comparison of the EZW measures with test images. (bpp=1.5)

measure	ext1		industry	
	original	smoothed	original	smoothed
IZ number	8311	6716	7777	6139
pages	18	15	18	16
times	6	7	6	7

the number of isolated zerotrees is decreased and accordingly the detected significant coefficients are scanned for more times.

From the above observations, we see that the changes of all these measures are consistent with our previous discussion. Thus, we can conclude that the proposed selective soft-thresholding method can smooth speckle noise and enhance inter-pixel correlation. As a result, we can compress the de-speckled SAR images more effectively.

7.4 Tests on Multiple Rate Image Compression

The purpose of the multiple rate scheme is to assign more bit budget to encode highlighted regions with more accuracy and spend only a small amount of bits to represent the background. Basically, it is difficult to tell how much information is adequate to represent the background or what ratio between the bit budgets for the two regions is appropriate for a particular application. Therefore, in this part, we will arbitrarily set some small bit rates and demonstrate how the multi-rate compression scheme works for SAR images. Since the highlighted region(s) will be encoded with more bits in the multi-rate case than in the flat rate case, the representation accuracy is definitely higher. Thus we will mainly evaluate this scheme by the visual quality of the reconstructed images rather than those quantitative measures.

The mask shown in Fig. 6.1 is used to specify two different resolutions for the original *industry* image. Fig. 7.10-(a) and (b) shows the images which result from the flat rate scheme and the multi-rate scheme, respectively. The bit budgets used in these two schemes are approximately the same. Fig. 7.10 is reconstructed with bpp=.43. We see it is highly distorted with much loss of information. In Fig. 7.10-(b), we see the highlighted region is still well represented (bpp=1.5) with acceptable visual quality. Fig. 7.10-(c) and (d) shows the error images of (a) and (b) as compared with the source image (shown in Fig. 4.1-(b)). We conclude that the highlighted region is better

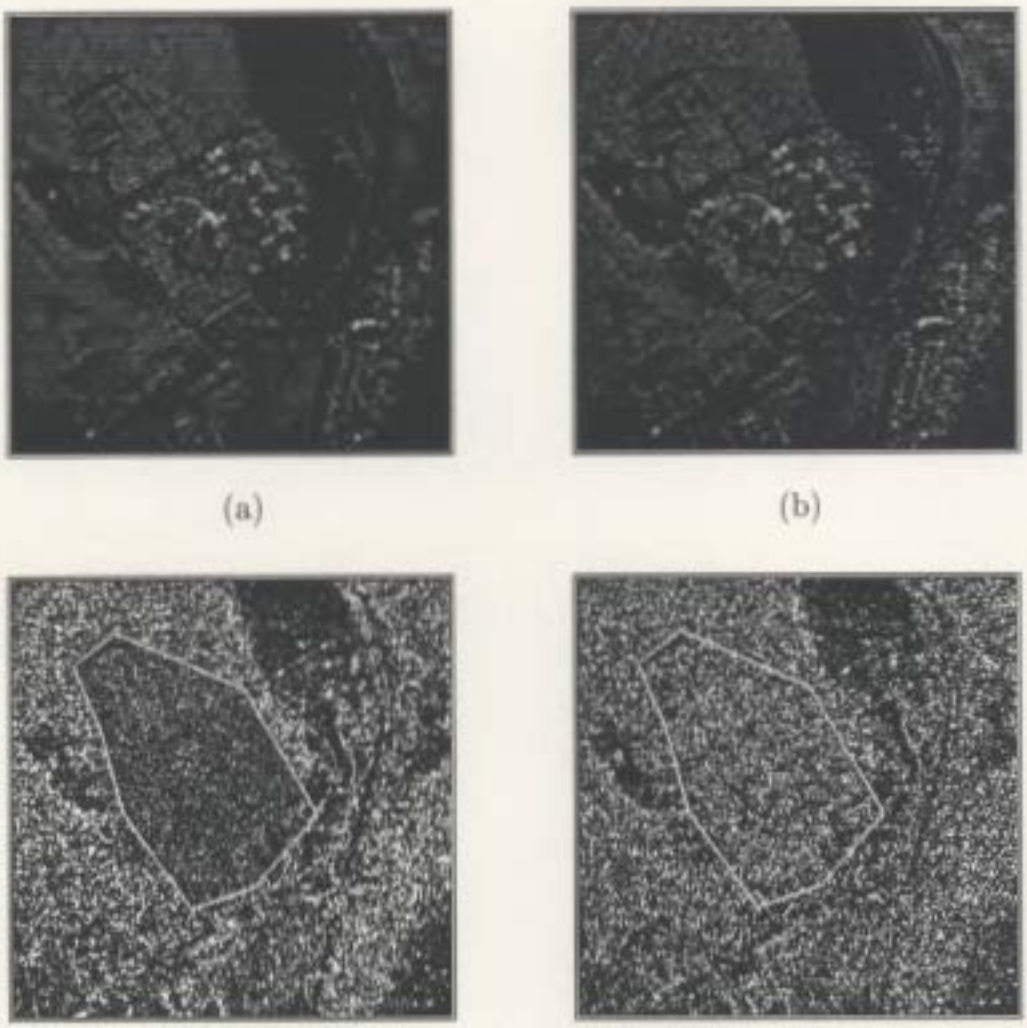

(a) (b)

(c) (d)

Figure 7.10: Multi-rate and flat rate reconstruction for original *industry* image. (a) multi-rate, interim bpp=1.5, external bpp=.13; (b) flat rate bpp=.43. (c) error image of (a) (offset multiplied by 3); (d) error image of (b) (offset multiplied by 3).

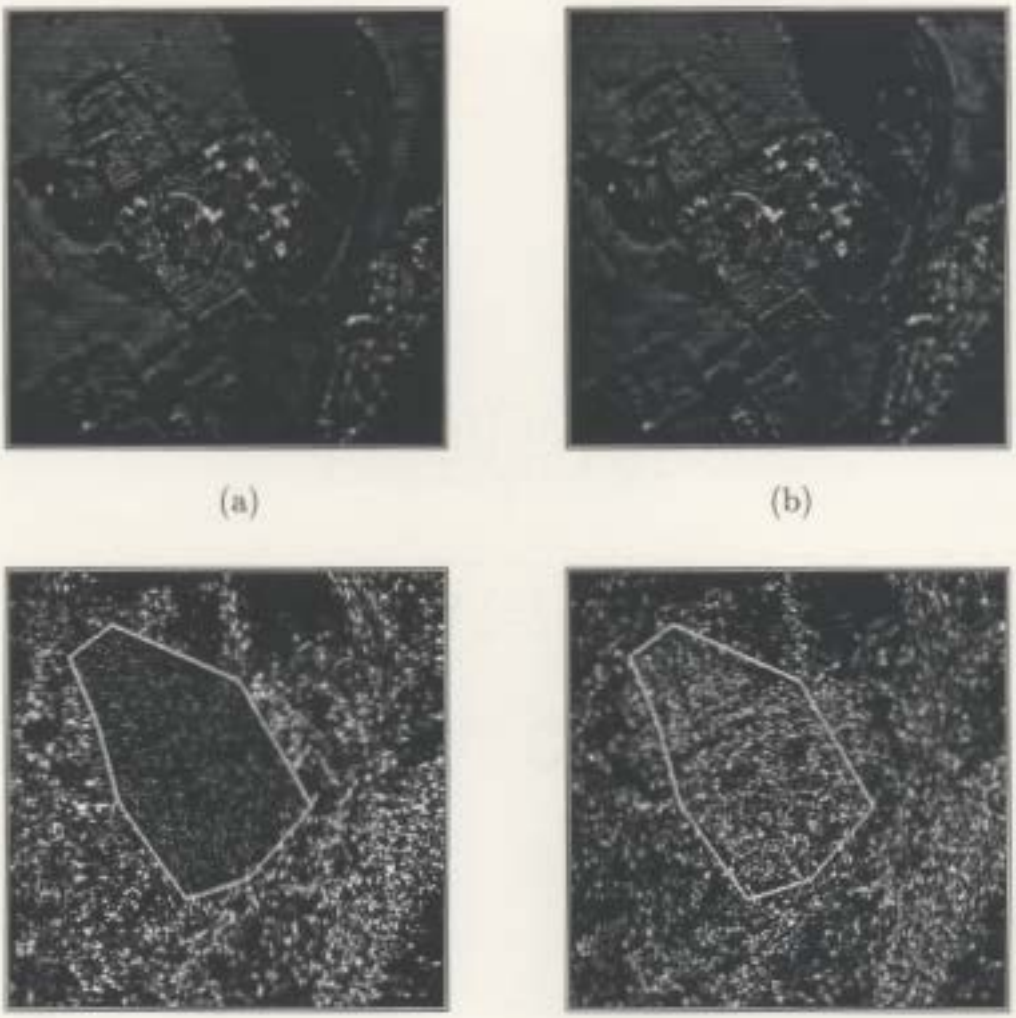

Figure 7.11: Multi-rate and flat rate reconstruction for de-speckled *industry* image. (a) multi-rate, interim bpp=1.5, external bpp=.13; (b) flat rate bpp=.43. (c) error image of (a) (offset multiplied by 3); (d) error image of (b) (offset multiplied by 3).

represented at the loss of blurred background.

Fig. 7.11 gives the images which result using the same parameters, but the source image is the de-speckled *industry* (shown in Fig. 7.1). We see that in this case both the highlighted and the background regions have better visual qualities due to the effect of speckle smoothing. This again demonstrates the effects of speckle reduction. But for the background regions, the two reconstructed images have similar visual qualities. This is because at very low bit rates, both speckle noise corrupted pixels and fine details are not encoded. Only major structures are encoded and transmitted.

The application of the multi-rate compression scheme, together with many issues about its implementation, such as the generation of the region masks, the specifications of the region parameters and the bit budget assignment strategy, is recommended for future research. Currently we find it is useful for images, and especially for large image browsing purposes. It may have some other applications, such as the monitoring of a moving target where the target itself is the major focus, but for which people may hope to collect some information about the surrounding areas. Tests in this section have demonstrated the effectiveness of the multi-rate compression scheme supported by wavelet domain region partitioning. Clearly more effort is required to answer further questions.

Chapter 8

Conclusions

The purpose of this thesis was to develop methods for SAR image compression. A primary requirement of such methods is that they should take into account the characteristics of SAR images which are different from optical images. Therefore, we need to adopt approaches specifically for SAR images to achieve the goal of SAR compression.

In this thesis, the problem of SAR speckle reduction and compression have been related and studied simultaneously. Although traditionally these two topics have been studied separately, we have placed these two topics in one framework in this thesis and have highlighted their inter-connection. In addition to its role in image compression, the wavelet transform also serves as an image processing tool and has produced promising speckle smoothing results. The main contributions of the thesis are listed below as results and observations.

The main results of the thesis are summarized below:

1. In examining the effect of speckle noise on SAR image compression, we have found that speckle noise tends to break the inter-pixel correlation in SAR images. As a result, algorithms which are successfully used for optical image compression perform less effectively for SAR images. Performance measures which characterize the run-length based and tree-structured compression algorithms are defined and evaluated. It has been found that speckle noise has more direct influence on run-length based algorithms. Thus, tree-structured compression algorithms, such as EZW, are recommended for SAR image compression.

2. A wavelet domain speckle smoothing method is proposed. The wavelet coefficient soft-thresholding method is an effective way to remove noise. In order to better preserve edge information, hierarchical correlation is introduced which exploits both the short term inter- band and intra-band correlation among the wavelet coefficients. According to this definition, only edge positions will have large correlation values. Therefore, we can protect these edge coefficients and only process other non-edge coefficients with soft-thresholding. By this means, simultaneous noise smoothing and edge preservation can be achieved.

3. A multi-rate compression scheme is implemented for browsing large SAR images. This scheme partitions an image into several regions in the wavelet domain. Each region is assigned a different bit budget according to the relative importance of the information each region

contains. A highlighted region can be encoded with higher accuracy and only the major structures in the background regions transmitted. Significant savings of communication resources can thus be expected.

The proposed noise smoothing and multi-rate compression scheme are applied to both synthetic speckled and real SAR images. The following observations have been made:

1. The proposed speckle smoothing method can effectively remove noise in homogeneous areas and at the same time preserve edges. This method is especially capable of detecting and enhancing oriented edges in noisy images, but it does not perform equally well on edges with short durations, such as point targets. This speckle smoothing method has been compared with the well-known Lee multiplicative speckle filter, and the results are competitive.

2. The selective soft-thresholding processed SAR images are more compressible than the speckled ones. This is because the speckle filter removes the noise which breaks the inter-pixel correlation in the images, and due to the nature of the proposed speckle filter, both the inter- and intra- band correlation among wavelet coefficients are enhanced by this processing. Thus compression performance is improved.

3. The multi-rate compression scheme can be used to represent highlighted regions fairly well even at low flat bit rates. This scheme, when com-

bined with the selective soft-thresholding method, can provide better visual quality for the highlighted regions. Since the EZW algorithm reorders wavelet coefficients according to their importance, major structures in the background can be easily picked up while finer details and speckle noise corrupted coefficients are eliminated at low bpp.

This thesis reported our work on SAR image compression and noise smoothing using the wavelet transform. Although we have answered several important questions, the thesis also raises many interesting issues. Some of the possible directions of the future work are mentioned as follows:

1. The reported work demonstrates that the idea of the multi-rate compression scheme is possible and practical. Significant further effort is required to achieve the final goal. The generation and transmission of the region mask and the specifications of the region parameters are problems which need to be solved and addressed.

2. We may use other wavelet families or continuous wavelet transforms to do the speckle smoothing. We may hope to specify some explicit conditions to stop the iterative algorithm instead of the trial and error approach. Some well-defined criterion may also help us select more appropriate processing parameters.

3. The proposed speckle smoothing method makes use of the so-called hierarchical correlation to identify edges from noise. If we totally elimi-

nate the noisy coefficients as well as the lowest resolution approximation subimage, we may obtain an effective wavelet domain edge detector.

Finally, while this work demonstrates some beauties of the wavelet transform in SAR image compression and processing, we have reasons to believe that a vast world is behind it.

Bibliography

[1] M. Acheroy and J.M. Mangen, "Comparison between JPEG. Block Wavelet Transform and Progressive Wavelet Transform for the Compression of METEOSAT Image Data", *Report of Royal Military Academy*. Brussels. 1994.

[2] Edwards H. Adelson and Eero P. Simoncelli. "Subband Image Coding with Three-tap Pyramids". *Picture Coding Symposium 1990*. Cambridge. MA. U.S.A.

[3] A.N. Akansu and R.A. Haddad. *"Multiresolution Signal Decomposition"*. Boston: Academic Press, 1992.

[4] Marc Antonini, Michel Barlaud, Pierre Mathieu and Ingrid Daubechies, "Image Coding Using Wavelet Transform", *IEEE Trans. on Image Processing*, vol. 1, n.2, pp. 205–220, 1992.

[5] H.H. Arsenault and M. Leveque, "Combined Homomorphic and Local-statistics Processing for Restoration of Images Degraded by Signal-dependent Noise", *Applied Optics*, vol. 23, n.6, 1984.

[6] M.R. Azimi-Sadjad and S. Bannour, "Two Dimensional Adaptive Block Kalman Filtering of SAR Imagery", *IEEE Trans. on Geoscience and Remote Sensing*, vol. 29, n.5, pp. 742–753, 1991.

[7] M. Barnsley. *"Fractals Everywhere"*. Boston: Academic Press. Inc.. 1988.

[8] L. Boroczky, R. Fioravanti, S. Fioravanti and D.D. Giusto, "Speckle Noise Filtering in SAR Images Using Wavelets", *8th International Conference on Image Analysis*, San Remo, Italy, Sept. 1995.

[9] P. Burt and E. Adelson, "The Laplacian Pyramid as a Compact Image Code", *IEEE Trans on Communications*, vol. 31. n.3. 1983.

[10] C.Y. Chang, R. Kwok and J.C. Curlander, "Spatial Compression of Seasat SAR Imagery", *IEEE Trans. on Geoscience and Remote Sensing*, vol. 26, n.5, pp. 673–685, 1988.

[11] A. Cohen, I. Daubechies and J.C. Feauveau, "Biorthogonal Bases of Compactly Supported Wavelets", *AT&T Bell Laboratories Tech. Report*. 1992.

[12] T.R. Crimmins, "Geometric Filter for Speckle Reduction", *Applied Optics*, vol. 24, n. 10, pp. 1438–1443, 1985.

[13] J.C. Curlander and R.N. McDonough. *"Synthetic Aperture Radar: Systems and Signal Processing"*. Wiley Series in Remote Sensing. New York: John Wiley & Sons. Inc.. 1991.

[14] I. Daubechies. *"Ten Lectures on Wavelets"*, CBMS-NSF Regional Conference Series. SIAM. 1992.

[15] R.W. Dijkerman and R.R. Mazumder, "On the Correlation Structure of the Wavelet Coefficients of Fractional Brownian Motion". *IEEE Trans. on Information Theory*, vol. 40, n. 5, pp. 1609–1612, 1994.

[16] David L. Donoho, "De-noising by Soft-thresholding", *IEEE Trans. on Information Theory*, vol. 41, n. 3, pp. 613–626. March 1995.

[17] V.S. Frost, J.S. Stiles, K.S. Shanmugan and J.C. Holtzman. "A Model for Radar Images and Its Application to Adaptive Digital Filtering of Multiplicative noise". *IEEE Trans. on Pattern Analysis and Machine Intelligence*, vol. 4, n.2, pp. 157–166, 1982.

[18] S. Foucher, G.B. Benie and J. Boucher, "Unsupervised Multiscale Speckle Filtering". *Proceedings of the International Conference on Image Processing*, pp. 391–394, 1996.

[19] L. Gagnon and F.D. Smaili, "Speckle Noise Reduction of Airborne SAR Images with Symmetric Daubechies Wavelets", *SPIE Symposium on Signal and Data Processing of Small Targets*, Orlando, FL. 1996.

[20] S.S. Ganugapati and C.R. Moloney, "A Ratio Based Edge Detector for Speckled Image Based on Maximum Strength Edge Pruning" *Proceedings of ICIP-95*, vol. II, pp. 165–168, Washington, D.C., October 1995.

[21] J.W. Goodman, "Some Fundamental Properties of Speckle", *J. Opt. Soc. Am.* vol. 66, n.11, pp. 1145–1150, 1976.

[22] A. Gersho and R.M. Gray, *"Vector Quantization and Signal Compression"*, Boston: Kluwer Academic Publishers, 1992.

[23] C. Ju and C. R. Moloney, "An Edge-Enhanced Modified Lee Filter for the Smoothing of SAR Image Speckle Noise", accepted for presentation on *1997 IEEE/EURASIP Workshop on Nonlinear Signal and Image Processing*, September 8–10, 1997, Mackinac Island, Michigan USA.

[24] D.T. Kuan, A. A. Sawchuk, T. C. Strand and P. Chavel, "Adaptive Noise Filter for Images with Signal-dependent Noise", *IEEE Trans. on Pattern Analysis and Machine Intelligence*, vol. 7, n.2, pp. 165–177, 1985.

[25] J.S. Lee,, "Digital image enhancement and noise filtering by use of local statistics", *IEEE Trans. on Pattern Analysis and Machine Intelligence*, vol. 2, pp. 165–168, 1980.

[26] J.S. Lee, "Speckle Analysis and Smoothing of SAR Images", *Computer Graphics and Image Processing*, vol. 17, pp. 24–32, 1981.

[27] J.S. Lee. "Refined Filtering of Image Noise Using Local Statistics". *Computer Vision. Graphics and Image Processing.* vol. 15. pp. 380–389. 1981.

[28] J.S. Lee. "A Simple Speckle Smoothing Algorithm for SAR Images". *IEEE Trans. on System. Man and Cybernetics.* vol. 13. n.1. pp. 85–89. 1983.

[29] Y. Li and C. R. Moloney, "SAR Image Compression Using Wavelet Transform and Soft-thresholding", *Proceedings of Canadian Conference on Electrical and Computer Engineering*, vol.1, pp. 387–390, 1997.

[30] Y. Li and C. R. Moloney, "Selective Wavelet Coefficient Soft-Thresholding Scheme for Speckle Noise Reduction in SAR Images". accepted for presentation at the *1997 IEEE/EURASIP Workshop on Nonlinear Signal and Image Processing.* September 8–10. 1997. Mackinac Island, Michigan USA.

[31] A. Lopes, R. Touzi and E. Nezry, "Adaptive Speckle Filters and Scene Heterogeneity", *IEEE trans. on Geoscience and Remote Sensing*", vol. 28. n.6, pp. 992–1000, 1990.

[32] S. Mallat, "A Theory for Multiresolution Signal Decomposition: The Wavelet Representation", *IEEE Trans. on Pattern Analysis and Machine Intelligence*, vol.11, n. 7, p. 674–693, 1989.

[33] S. Mallat and W.L. Hwang. "Singularity Detection and Processing with Wavelet". *IEEE Trans. on Information Theory*. vol. 38. n. 2. pp. 617–643. 1992.

[34] C.R. Moloney. "Smoothing of SAR Image Speckle Noise by Multiplicative Point Estimation Filters". *Proceedings of ICIP-96*. vol. III. pp. 970–910. Lausanne, Switzerland, September 1996.

[35] D. C. Munson, Jr. and R. L. Visentin, "A Signal Processing View of Strip-Mapping Synthetic Aperture Radar", *IEEE Trans. on Acoustic. SPeech and Signal Processing*, vol. 37. n.12, pp. 2131–2147. 1989.

[36] J.E. Odegard. H. Guo. M. Lang. C.S. Burrus and R.O. Wells. Jr.. "Wavelet based SAR Speckle Reduction and Image Compression". *SPIE Symposium on OE/Aerospace Sensing and Dual Use Photonics*. April 1995.

[37] W. K. Pratt, *Digital Image Processing*, New York: Wiley, 1978.

[38] G. Ramponi and C.R. Moloney. "Smoothing Speckled Images Using An Adaptive Rational Operator", *IEEE Signal processing Letters*. vol. 4. n.3, pp. 68–71, 1997.

[39] J. R. Robinson, "Efficient General-purpose Image Compression With Binary-tree Predictive Coding", *IEEE Trans. on Image Processing*. vol. 6, n. 4, pp. 601–608, 1997.

[40] R.E. Roger and J.F. Arnold, "Reversible Image Compression Bounded by Noise", *IEEE Trans. on Geoscience and Remote Sensing*, vol. 32, n.1, pp. 19–24, 1994.

[41] F. Safa and G. Flouzat, "Speckle Removal on Radar Imagery Based on Mathematical Morphology", *Signal Processing*, vol. 16, pp. 319–333, 1989.

[42] A. Said and W.A. Pearlman, "A New Fast and Efficient Image Codec Based on Set Partitioning in Hierarchical Trees", *IEEE Trans. on Circuits and Systems for Video Technology*, vol. 6, n.3, pp. 243–250, 1996.

[43] N.D. Memon, K. Sayood and S.S. Magliveras, "Lossless Compression of Multispectral Image Data", *IEEE Trans. on Geoscience and Remote Sensing*, vol. 32, n.2, pp. 282–289, 1994.

[44] Jarome M. Shapiro, " Embedded Image Coding Using Zerotree of Wavelet Coefficients", *IEEE Trans. on Signal Processing*, vol. 41, No. 12, pp. 3445–3462, December 1993.

[45] C. M. Thompson and L. Shure, *"Image Processing Toolbox"*, The MathWorks, Inc., 1993.

[46] M. Tur, K.C. Chin and J.W. Goodman, "When Is Speckle Noise Multiplicative", *Applied Optics*, vol.21, n.7, pp. 1157–1159, 1982.

[47] F.T. Ulaby, T.F. Haddock and R.T. Austin, "Fluctuation Statistics of Millimeter-wave Scattering from Distributed Targets", *IEEE Trans. on Geoscience and Remote Sensing*, vol. 26, n.3, pp. 268–281, 1988.

[48] M. Vetterli and J. Kovacevic, "*Wavelet and Subband Coding*", Prentice Hall, Inc., 1995.

[49] John D. Villasenor, Benjamin Belzer and Judy Liao, "Wavelet Filter Evaluation for Image Compression", *IEEE Trans. on Image Processing*, vol. 4, No. 8, pp. 1053–1060, 1995.

[50] G.K. Wallace, "The JPEG Still Picture Compression Standard", *Communications of the ACM*, vol. 34, n.4, pp. 31–91, 1991.

[51] J. Wang, K. Zhang and S. Tang, "Spectral and Spatial Decorrelation of Landsat-TM Data for Lossless Compression", *IEEE Trans. on Geoscience and Remote Sensing*, vol. 33, n.5, pp. 1277–1285, 1995.

[52] S. Ward, "Digital Image Processing of Airborne Side-looking Synthetic Aperture Radar", *NSERC USRA report*, Memorial University of Newfoundland, St. John's, NF, Canada, 1993.

[53] J. Way and E. A. Smith, "The Evolution of Synthetic Aperture Radar System and Their Progression to the EOS SAR", *IEEE Trans. on Geoscience and Remote Sensing*, vol. 29, n. 6, pp. 962–985, 1991.

[54] X. Wu. "Image Coding by Adaptive Tree-structure Segmentation". *IEEE Trans. on Information Theory*, vol. 38, n.6, pp. 1755–1767, 1992.

[55] Y. Xu, J.B. Weaver, D.M. Healy, Jr. and J. Lu. "Wavelet Transform Domain Filters: A Spatially Selecitve Noise Filtration Technique". *IEEE Trans. on Image Processing*, vol. 3, n.6, pp. 747–758, 1994.

[56] website, *http://www.nasoftware.co.uk/SAR/what_is_sar.html*, March 2, 1997.

[57] website, *http://sdcd.gsfc.nasa.gov/GRSS/Data_Comp*, Feb 12, 1996.

[58] EPIC source code, ftp site *maxwell.math.sc.edu*, under directory */pub/wavelet/archive*, 1989.

[59] EZW source code, ftp site: *ftp rpi.edu*, under directory */pub/wavelet/EZW*, 1992.

IMAGE EVALUATION TEST TARGET (QA-3)

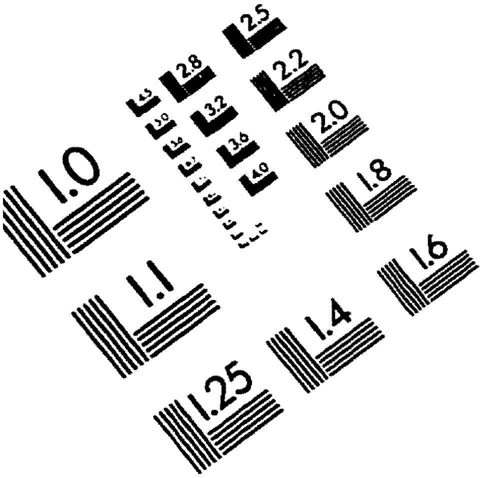

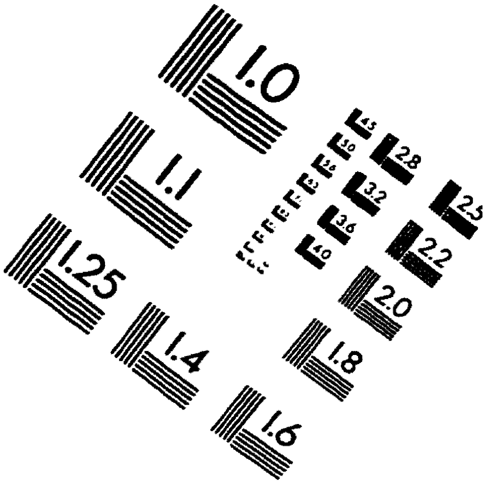

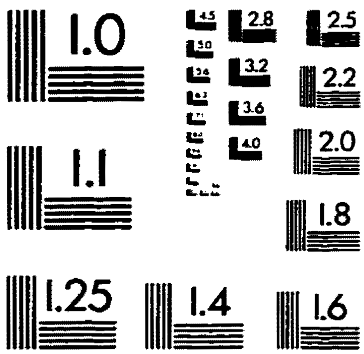

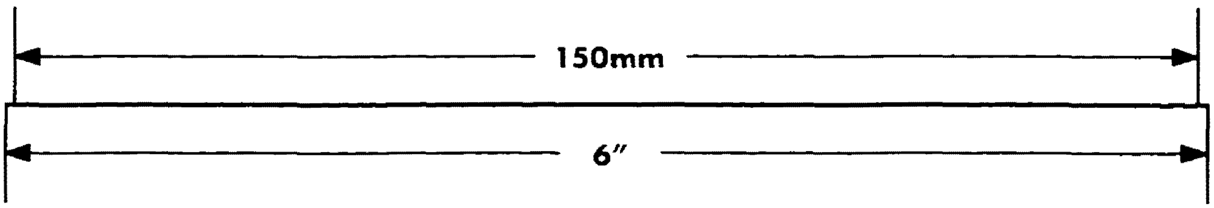

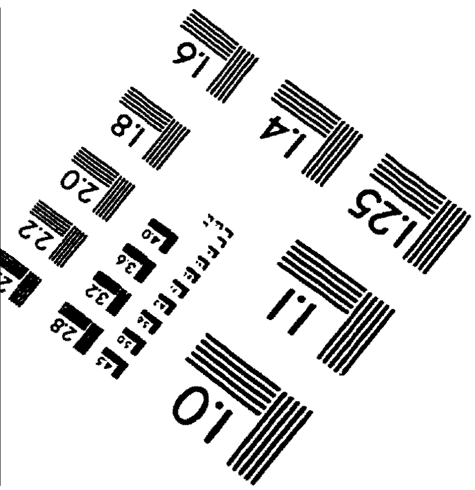

APPLIED IMAGE, Inc
1653 East Main Street
Rochester, NY 14609 USA
Phone: 716/482-0300
Fax: 716/288-5989